

Recurrent neural chemical reaction networks that approximate arbitrary dynamics

Alexander Dack^{*,1} Benjamin Qureshi¹ Thomas E. Ouldridge¹ Tomislav Plesa^{*,2}

Keywords: Chemical Reaction Networks; Artificial Neural Networks; Dynamical Systems

Abstract: Many important phenomena in biochemistry and biology exploit dynamical features such as multi-stability, oscillations, and chaos. Construction of novel chemical systems with such rich dynamics is a challenging problem central to the fields of synthetic biology and molecular nanotechnology. In this paper, we address this problem by putting forward a molecular version of a recurrent artificial neural network, which we call *recurrent neural chemical reaction network* (RNCRN). The RNCRN uses a modular architecture – a network of chemical neurons – to approximate arbitrary dynamics. We first prove that with sufficiently many chemical neurons and suitably fast reactions, the RNCRN can be systematically trained to achieve any dynamics. RNCRNs with relatively small number of chemical neurons and a moderate range of reaction rates are then trained to display a variety of biologically-important dynamical features. We also demonstrate that such RNCRNs are experimentally implementable with DNA-strand-displacement technologies.

1 Introduction

Artificial neural networks (ANNs) are a set of algorithms, inspired by the structure and function of the brain, that are commonly implemented on electronic machines [1]. Owing to their powerful function approximating abilities [2–4], ANNs have been used to solve a range of data-driven problems involving identification, prediction and classification of patterns, e.g. in text, speech and image analysis [5]. These networks, and particularly their recurrent counterparts [6–8], have also been embedded into dynamical systems [9] to learn arbitrary dynamical behaviors [10, 11], including oscillations [12] and chaos [13, 14].

ANNs implemented on electronic machines can be challenging to interface with chemical and biological systems. To address this issue, as done with some other chemically-realized systems [15–21], there has been substantial interest in directly embedding ANNs into *chemical reaction networks* (CRNs) - a mathematical framework used for modelling (bio)chemical processes [22]. In this paper, such CRNs, that execute ANN algorithms, are said to be *neural*. Current literature has focused on designing neural CRNs to solve various pattern-recognition problems [23–38], with applications to e.g. virus detection [27] and disease diagnostics [38], with successful experimental implementations using substrates such as nucleic acids and microorganisms [38–42]. Particular focus has been placed on both theoretical investigations [27, 29, 37, 42] and experimental implementations [36, 42] of neural CRNs based on the classical architecture consisting of layers of perceptrons - processing units whose outputs are non-linear functions of weighted sum of their inputs [43].

The neural CRNs put forward in the literature for molecular pattern-recognition problems take an input set of chemical concentrations and produce in the long-run *static* (equilibrium)

* Email of co-corresponding authors: alex.dack14@imperial.ac.uk or tp525@cam.ac.uk.

¹Department of Bioengineering and Imperial College Centre for Synthetic Biology, Imperial College London, Exhibition Road, London, SW7 2AZ, UK.

²Department of Applied Mathematics and Theoretical Physics, University of Cambridge, Centre for Mathematical Sciences, Wilberforce Road, Cambridge, CB3 0WA, UK.

concentrations as the output. As such, these CRNs cannot in general be trained to produce a predefined *dynamical* (non-equilibrium) output. However, it is precisely the dynamical signals that can communicate important messages in biology. In particular, the time-evolution of (bio)chemical species concentrations can be modelled as a dynamical system [9, 22], and the detailed information encoded in this time-evolution can play important roles in biology [44]. For example, fundamental processes such as cellular differentiation, circadian clocks and DNA repair have been modelled as dynamical systems that exhibit features such as coexistence of multiple favorable states (multi-stability) and oscillations [45–47]. Furthermore, chaotic dynamical systems have been used to explain survival advantage of cellular populations [48], and heterogeneity in bacterial responses to stress [49]. Aside from occurring in native (bio)chemical systems, such dynamical features have also been encoded in a variety of experimentally-built synthetic ones. Examples include DNA-strand-displacement systems that display oscillations [50] and process temporal information [51], enzyme-aided DNA systems displaying oscillations, chaos, spiking, and molecular event recording [52–54], synthetic gene-regulatory networks displaying oscillations [55], all the way to multi-stable synthetic bacteria [56].

One class of neural systems, which can be suitable for dynamical problems, are *chemical reservoir computers* [57, 58]. These chemical-electronic hybrid systems consist of a suitable CRN (called the chemical reservoir) which is coupled to a single layer implemented on an electronic computer. The authors from [58] choose a particular CRN with rich dynamics, and demonstrate that the chemical reservoir computer can then solve a number of computational problems, including emulating and predicting dynamical systems. To achieve these tasks, only a single layer is trained, which is less computationally intensive than the classical training of ANNs. However, these chemical reservoir computers have not been shown to possess the ability to replicate arbitrary dynamical behaviors and, furthermore, they are not purely chemical, relying on an electronic computer.

To bridge the gap, in this paper we introduce a family of novel (purely chemical) neural CRNs that can replicate arbitrary dynamical behaviors. These CRNs embed suitable perceptron-based recurrent ANNs, and are called *recurrent neural chemical reaction networks* (RNCRNs). The RNCRNs contain two types of chemical species: the *executive* species, that execute the desired dynamics, and chemical analogues of perceptrons [29], called the *chemical perceptrons*, that fine-tune the dynamics of the executive species in a recurrent-neural-network fashion; see Figure 1 for a schematic representation. By exploiting the universal approximation abilities of ANNs, we prove that RNCRNs can be systematically trained to achieve dynamics of any well-behaved target dynamical system, provided that there are sufficiently many chemical perceptrons, and provided that these species are governed by sufficiently fast reactions. We show that non-trivial dynamical behaviors can be replicated with relatively few and only moderately fast chemical perceptrons. Furthermore, we demonstrate that RNCRN-based systems can be implemented under experimentally-feasible conditions using DNA-strand-displacement technologies.

The paper is organized as follows. In Section 2, we present background theory on CRNs and ANNs. In Section 3, we introduce RNCRNs, and outline their universal approximation abilities, which are rigorously proved in Appendix A. In Section 4, we present an algorithm for training RNCRNs as Algorithm 1, which we apply to obtain relatively simple RNCRNs displaying multi-stability, oscillations, and chaos; more details about the examples can be found in Appendix B, while the pseudocode for Algorithm 1 in Appendix F. In addition, in Appendices C and D, we study some experimentally-important properties of some of the example systems. Finally, we provide a summary and discussion in Section 5; some further details can be found in Appendix E.

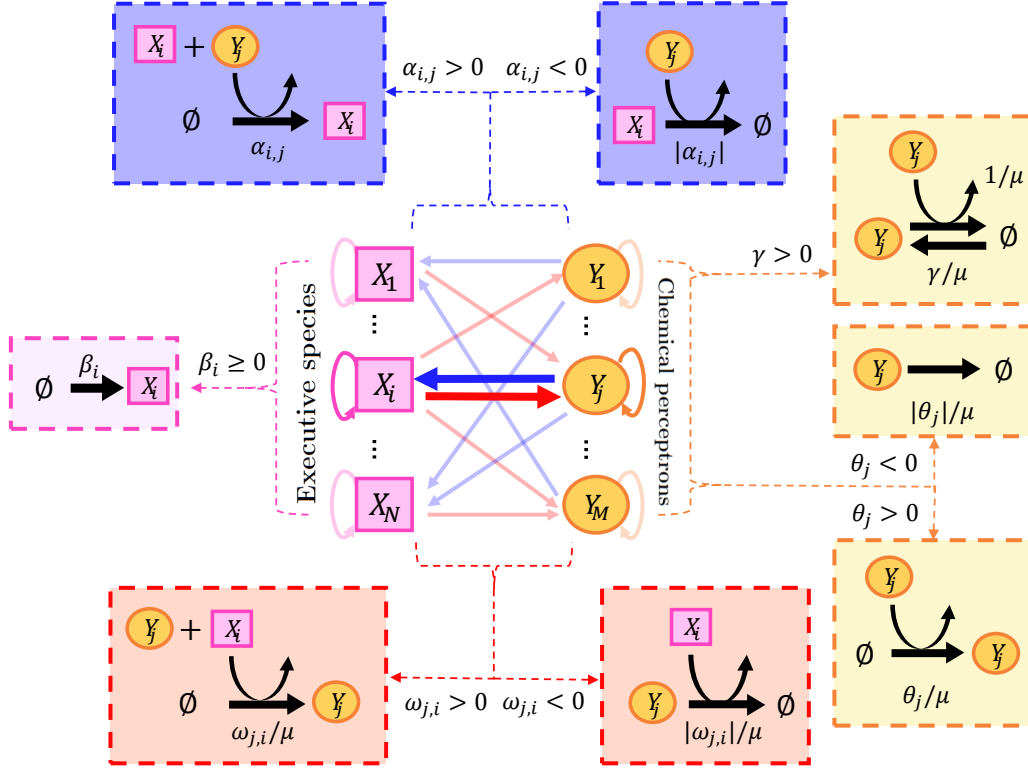


Figure 1: A visualization of an RNCRN with executive species X_1, X_2, \dots, X_N , and a single layer of chemical perceptrons Y_1, Y_2, \dots, Y_M . The interaction between the executive species and chemical perceptrons is outlined in the center via arrows, while the surrounding boxes display more details. In particular, the purple box on the left displays chemical reactions that involve only the executive species; similarly, the yellow boxes on the right show reactions only involving the chemical perceptrons; here, black curved arrows indicate catalysis. On the other hand, the boxes on the top and bottom display reactions that involve both types of species; these interactions are catalytic in nature. In particular, shown in blue on the top are the reactions affecting the executive species, where the chemical perceptrons are catalysts; on the other hand, the orange boxes on the bottom display reactions which affect the chemical perceptrons, with executive species being catalysts. The corresponding chemical reaction network is given by (14) in Appendix A; see also Table 1.

2 Background theory

In this section, we present some theory of chemical reaction networks and artificial neural networks. Throughout the paper, we assume that all the variables are dimensionless, unless stated otherwise.

2.1 Chemical reaction networks (CRNs)

Consider a system of two ordinary-differential equations (ODEs) given by

$$\frac{dx}{dt} = \beta + \alpha xy, \quad \frac{dy}{dt} = \gamma + \theta y + \omega xy - y^2. \quad (1)$$

Let us assume that the real (dimensionless) parameters $\beta, \gamma > 0$ are positive, while $\alpha, \theta, \omega \in \mathbb{R}$ can be either positive or negative. Then, dynamical system (1) is an example of *reaction-rate equations*

(RREs) - ODEs that model time-evolution of concentrations of chemical species under suitable conditions [22]. In particular, $x = x(t) \geq 0$ and $y = y(t) \geq 0$ satisfying RREs (1) can be interpreted as (dimensionless) concentrations of some chemical species X and Y at time $t \geq 0$, respectively.

Chemical reactions. Each term on the right-hand side of the RREs (1) can be interpreted as the rate of a chemical reaction, which we summarize in Table 1. For example, the term $\beta > 0$ from (1) can be interpreted as the rate of the reaction $\emptyset \xrightarrow{\beta} X$, which describes a production of species X from some species which we do not explicitly model, and denote by \emptyset . On the other hand, no chemical reaction can be associated to the term $\beta < 0$ [59]. This information is summarized in the first row of Table 1. Similarly, in the second row and second column, it is shown that the term αxy from (1) can be interpreted as the rate of $X + Y \xrightarrow{\alpha} 2X + Y$ if $\alpha > 0$. According to this reaction, when species X and Y react, one molecule of X is produced. Since then the molecular count of Y remains unchanged, we say that Y is a *catalyst* in the reaction. On the other hand, as presented in the second row and third column of Table 1, when $\alpha < 0$, the term αxy can be interpreted as the rate of $X + Y \xrightarrow{|\alpha|} Y$, where $|\alpha|$ denotes the absolute value of α . According to this reaction, when X and Y react, one molecule of X is degraded with Y being a catalyst.

Table 1: Chemical reactions induced by RREs (1).

Term in RREs (1)	Reaction for positive term	Reaction for negative term
β	$\emptyset \xrightarrow{\beta} X$	Never negative
αxy	$X + Y \xrightarrow{\alpha} 2X + Y$	$X + Y \xrightarrow{ \alpha } Y$
γ	$\emptyset \xrightarrow{\gamma} Y$	Never negative
θy	$Y \xrightarrow{\theta} 2Y$	$Y \xrightarrow{ \theta } \emptyset$
ωxy	$X + Y \xrightarrow{\omega} X + 2Y$	$X + Y \xrightarrow{ \omega } X$
$-y^2$	Never positive	$2Y \xrightarrow{1} Y$

The correspondence between RREs (1) and the chemical reactions, shown in Table 1, is called *mass-action kinetics* [22]: the rate of a reaction is given by the product of the concentrations of the reactants (species on the left-hand side of the reaction) multiplied by the *rate coefficient* - the positive number displayed above the reaction arrow. Let us note that the rate coefficient in $-y^2$ from (1) is fixed to 1, and this term is never positive, as summarized in the final row of Table 1. Systems of chemical reactions, such as those presented in Table 1, are called *chemical reaction networks* (CRNs) under mass-action kinetics [22]. In this paper, we denote the chemical species by $X_1, X_2, \dots, Y_1, Y_2, \dots$, their concentrations by respectively $x_1, x_2, \dots, y_1, y_2, \dots$, and the rate coefficients of the underlying reactions by $\alpha, \beta, \gamma, \theta, \omega$ with appropriate subscripts; additional symbols are introduced when we consider experimental implementations of CRNs.

Experimental implementation. In this paper, we focus on the mass-action chemical reactions of the form given in Table 1. All of these reactions have at most two reactants; consequently, the induced RREs have quadratic polynomials on the right-hand side, as in (1). However, let us stress that the abstract reactions from Table 1 cannot be experimentally implemented in their original form; for example, $\emptyset \rightarrow X_1$ cannot be implemented as it contains a non-specific species \emptyset , while $X + Y \rightarrow 2X + Y$ cannot be implemented as it describes a catalytic production as a single chemical step. Nevertheless, CRNs consisting of any number of the abstract reactions from Table 1, including reactions that have the same reactants, but different products, such as $X + Y \rightarrow 2X + Y$ and $X + Y \rightarrow Y$, can be approximated by experimentally implementable CRNs [60–64]. This

approximation is achieved by introducing into the abstract CRNs suitable additional chemical species and reactions. In particular, one possible implementation is via DNA strand-displacement [62, 63], or enzyme-aided DNA systems [64]. For more details, see Section 4.1 and Appendix C.

2.2 Artificial neural networks (ANNs)

Artificial neural networks (ANNs) are systems of connected processing units called artificial neurons. In this paper, we consider a particular type of artificial neurons called the *perceptron* [43]. Given a set of inputs, a perceptron first applies an affine function, followed by a suitable non-linear function, called the activation function, to produce a single output. More precisely, reusing some of the symbols from Section 2.1, let $x_1, x_2, \dots, x_N \in \mathbb{R}$ be the input values, $\omega_1, \omega_2, \dots, \omega_N \in \mathbb{R}$ the weights, $\theta \in \mathbb{R}$ a bias, and $\sigma : \mathbb{R} \rightarrow \mathbb{R}$ a suitable non-linear function. Then, the perceptron is a function $y : \mathbb{R}^N \rightarrow \mathbb{R}$ defined as

$$y(x_1, \dots, x_N) = \sigma \left(\sum_{j=1}^N \omega_j x_j + \theta \right). \quad (2)$$

Chemical perceptron. A natural question arises: is there a CRN with single species Y such that its RRE has a unique stable equilibrium of the form (2)? Such an RRE has been put forward and analysed in [29], and is given by

$$\frac{dy}{dt} = \gamma + \left(\sum_{j=1}^N \omega_j x_j + \theta \right) y - y^2, \quad (3)$$

where x_1, x_2, \dots, x_N are parameters. Since $\sum_{j=1}^N \omega_j x_j + \theta$ has a fixed sign, one can readily use Table 1 to write down a CRN corresponding to (3). We call the species Y with concentration y satisfying (3) a *chemical perceptron*. Setting the left-hand side in (3) to zero, one finds that the perceptron concentration has a globally stable equilibrium y^* , given by

$$y^* = \sigma_\gamma \left(\sum_{j=1}^N \omega_j x_j + \theta \right) \equiv \frac{1}{2} \left[\left(\sum_{j=1}^N \omega_j x_j + \theta \right) + \sqrt{\left(\sum_{j=1}^N \omega_j x_j + \theta \right)^2 + 4\gamma} \right]. \quad (4)$$

We call σ_γ with $\gamma > 0$ a *chemical activation function*. In this paper, we allow any $\gamma > 0$, but note that σ_γ approaches the rectified linear unit (ReLU) activation function in the special case as $\gamma \rightarrow 0$ [29], which is a common choice in the ANN literature [5].

3 Recurrent neural chemical reaction networks (RNCRNs)

Let us consider a *target* ODE system with initial conditions, given by

$$\frac{d\bar{x}_i}{dt} = f_i(\bar{x}_1, \dots, \bar{x}_N), \quad \bar{x}_i(0) = a_i \geq 0, \quad \text{for } i = 1, 2, \dots, N. \quad (5)$$

In what follows, we call the ODE right-hand side (f_1, f_2, \dots, f_N) a *vector field*, which we assume is sufficiently smooth. Without loss of generality, we assume that (5) has desirable dynamical features in the positive orthant $\mathbb{R}_{>}^N$. If such features are located elsewhere, a suitable affine change of coordinates can be used to move these features to the positive orthant [59].

We wish to find a neural CRN with some chemical species X_1, \dots, X_N whose concentrations approximate the solutions of the target ODEs (5). Inspired by the chemical perceptron (3), let us consider the RREs and initial conditions given by

$$\begin{aligned} \frac{dx_i}{dt} &= \beta_i + x_i \sum_{j=1}^M \alpha_{i,j} y_j, & x_i(0) &= a_i, \quad \text{for } i = 1, 2, \dots, N, \\ \frac{dy_j}{dt} &= \frac{\gamma}{\mu} + \frac{\theta_j}{\mu} y_j + \left(\sum_{i=1}^N \frac{\omega_{j,i}}{\mu} x_i \right) y_j - \frac{1}{\mu} y_j^2, & y_j(0) &= b_j, \quad \text{for } j = 1, 2, \dots, M. \end{aligned} \quad (6)$$

We call the CRN corresponding to the RREs (6) a *recurrent neural chemical reaction network* (RNCRN), and display it schematically in Figure 1. The RNCRN consists of two sub-networks: the executive system and the neural system. The executive system contains chemical reactions which directly change the *executive* species X_1, X_2, \dots, X_N . Note that the initial conditions for the executive species from (6) match the target initial conditions from (5). On the other hand, the neural system contains the reactions which directly influence the auxiliary species Y_1, Y_2, \dots, Y_M , for which we allow arbitrary initial conditions $b_1, b_2, \dots, b_M \geq 0$. These species can be formally identified as chemical perceptrons, see (3). However, let us stress that the RRE (3) depends on the *parameters* x_1, x_2, \dots, x_N . In contrast, the concentrations of chemical perceptrons from the RNCRN depend on the time-dependent executive *variables* $x_1(t), x_2(t), \dots, x_N(t)$, which in turn depend on the perceptron concentrations $y_1(t), y_2(t), \dots, y_M(t)$. In other words, there is a feedback between the executive and neural systems, giving the RNCRN a recurrent character. This feedback is catalytic in nature: the chemical perceptrons are catalysts in the executive system; similarly, executive species are catalysts in the neural system.

Main result: Universal approximation. We now wish to choose the parameters in the RNCRN so that the concentrations of the executive species $x_i(t)$ from (6) are close to the target variables $\bar{x}_i(t)$ from (5). Key to achieving this match is the parameter $\mu > 0$, which sets the speed at which the perceptrons equilibrate relative to the executive system. This speed can be formally set to be infinite by multiplying the RREs for the perceptrons in (6) by μ and then fixing $\mu = 0$. These RREs then become algebraic equations, whose solutions are given by $y_j^* = \sigma_\gamma(\sum_{i=1}^N \omega_{j,i} x_i + \theta_j)$, where σ_γ is of the form (4). We then say that the chemical perceptrons are in the *quasi-static* state. In this case, the executive species are governed by the *reduced* ODEs, given by

$$\frac{d\tilde{x}_i}{dt} = g_i(\tilde{x}_1, \dots, \tilde{x}_N) = \beta_i + \tilde{x}_i \sum_{j=1}^M \alpha_{i,j} \sigma_\gamma \left(\sum_{k=1}^N \omega_{j,k} \tilde{x}_k + \theta_j \right), \quad \tilde{x}_i(0) = a_i, \quad \text{for } i = 1, 2, \dots, N. \quad (7)$$

This reduced system allows us to prove that the RNCRN can in principle be fine-tuned to execute the target dynamics arbitrarily closely. In particular, to achieve this task, we follow two steps.

Firstly, we assume that the chemical perceptrons are in the quasi-static state, i.e. we consider the reduced system (7). Using the classical (static) theory from ANNs, it follows that the rate coefficients from the RNCRN can be fine-tuned so that the vector field from the reduced system (7) is close to that of the target system (5). To ensure a good vector field match, one in general requires sufficiently many chemical perceptrons. We call this first step the *quasi-static approximation*.

Secondly, we disregard the assumption that the chemical perceptrons are in the quasi-static state, i.e. we consider the full system (6). Nevertheless, we substitute into the full system the rate coefficients found in the first step. Using perturbation theory, it follows that, under this parameter choice, the concentrations of the executive species from the full system (6) approximate the dependent

variables from the target system (5) arbitrarily closely, provided that the chemical perceptrons fire sufficiently (but finitely) fast. We call this second step the *dynamical approximation*.

In summary, the RNCRN induced by (6) with sufficiently many chemical perceptrons ($M \geq 1$ large enough) which act sufficiently fast ($\mu > 0$ small enough) can execute any target dynamics. This universal approximation result is stated rigorously and proved in Appendix A.

4 Examples

In Section 3, we have outlined a two-step procedure used to prove that RNCRNs can theoretically execute any desired dynamics. Aside from being of theoretical value, these two steps also form a basis for a practical method to train RNCRNs, which is presented as Algorithm 1. In this section, we show that Algorithm 1 can be used to train RNCRNs with a relatively small number of perceptrons M and moderate perceptron speed μ to achieve predefined multi-stability, oscillations, and chaos.

Fix a target system (5) and target compact sets $\mathbb{K}_1, \mathbb{K}_2, \dots, \mathbb{K}_N \subset (0, +\infty)$. Fix also the rate coefficients $\beta_1, \beta_2, \dots, \beta_N \geq 0$ and $\gamma > 0$ in the RNCRN system (6).

- (a) **Quasi-static approximation.** Fix a tolerance $\varepsilon > 0$. Fix also the number of perceptrons $M \geq 1$. Using the backpropagation algorithm [65], find the coefficients $\alpha_{i,j}^*, \theta_j^*, \omega_{j,i}^*$ for $i = 1, 2, \dots, N$, $j = 1, 2, \dots, M$, such that (mean-square) distance between $(f_i(x_1, x_2, \dots, x_N) - \beta_i)/x_i$ and $\sum_{j=1}^M \alpha_{i,j}^* \sigma_\gamma \left(\sum_{k=1}^N \omega_{j,k}^* x_k + \theta_j^* \right)$ is within the tolerance for $(x_1, x_2, \dots, x_N) \in \mathbb{K}_1 \times \mathbb{K}_2 \times \dots \times \mathbb{K}_N$. If the tolerance ε is not met, then repeat step (a) with $M + 1$.
- (b) **Dynamical approximation.** Substitute $\alpha_{i,j} = \alpha_{i,j}^*$, $\theta_j = \theta_j^*$, $\omega_{j,i} = \omega_{j,i}^*$ into the RNCRN (6). Fix the initial conditions $a_1, a_2, \dots, a_M \geq 0$, $b_1, b_2, \dots, b_M \geq 0$, and time $T > 0$. Fix also the speed $0 < \mu \ll 1$ of the perceptrons. Numerically solve the target system (5) and the RNCRN system (6) over the desired interval $[0, T]$. Time $T > 0$ must be such that $\bar{x}_i(t), x_i(t) \in \mathbb{K}_i$ for all $t \in [0, T]$ for $i = 1, 2, \dots, N$. If $\bar{x}_i(t)$ and $x_i(t)$ are sufficiently close according to a desired criterion for all i , then terminate the algorithm. Otherwise, repeat step (b) with a smaller μ . If no desirable μ is found, then go back to step (a) and choose a smaller ε .

Algorithm 1: *Two-step algorithm for training the RNCRN. See Appendix F for pseudocode.*

4.1 Multi-stability

Let us consider the one-variable target ODE

$$\frac{d\bar{x}_1}{dt} = f_1(\bar{x}_1) = \sin(\bar{x}_1), \quad \bar{x}_1(0) = a_1 \geq 0. \quad (8)$$

This system has infinitely many equilibria, which are given by $\bar{x}_1^* = n\pi$ for integer values of n . The equilibria with even n are unstable, while those with odd n are stable.

Bi-stability. Let us now apply Algorithm 1 on the target system (8), in order to find an associated bi-stable RNCRN. In particular, let us choose the target region to be $\mathbb{K}_1 = [1, 12]$, which includes two stable equilibria, π and 3π , and one unstable equilibrium, 2π . We arbitrarily fix the free rate coefficients to $\beta_1 = 0$ and $\gamma = 1$.

(a) *Quasi-static approximation.* Let us apply the first step from Algorithm 1. We find that the tolerance $\varepsilon \approx 10^{-3}$ can be met with $M = 3$ chemical perceptrons, if the rate coefficients $\alpha_{1,j}, \theta_j, \omega_{j,1}$ in the reduced ODE (7) are chosen as follows:

$$\begin{aligned} \frac{d\tilde{x}_1}{dt} = g_1(\tilde{x}_1) = & -0.983\sigma_1(-1.167\tilde{x}_1 + 7.789)\tilde{x}_1 \\ & - 0.050\sigma_1(0.994\tilde{x}_1 - 1.918)\tilde{x}_1 \\ & + 2.398\sigma_1(-0.730\tilde{x}_1 + 3.574)\tilde{x}_1. \end{aligned} \quad (9)$$

In Figure 2(a), we display the vector fields of the target (8) and reduced system (9). One can notice an overall good match within the desired set $\mathbb{K}_1 = [1, 12]$, shown as the unshaded region. As expected, the approximation is poor outside of \mathbb{K}_1 ; furthermore, for the given tolerance, the accuracy is also reduced near the right end-point of the target set.

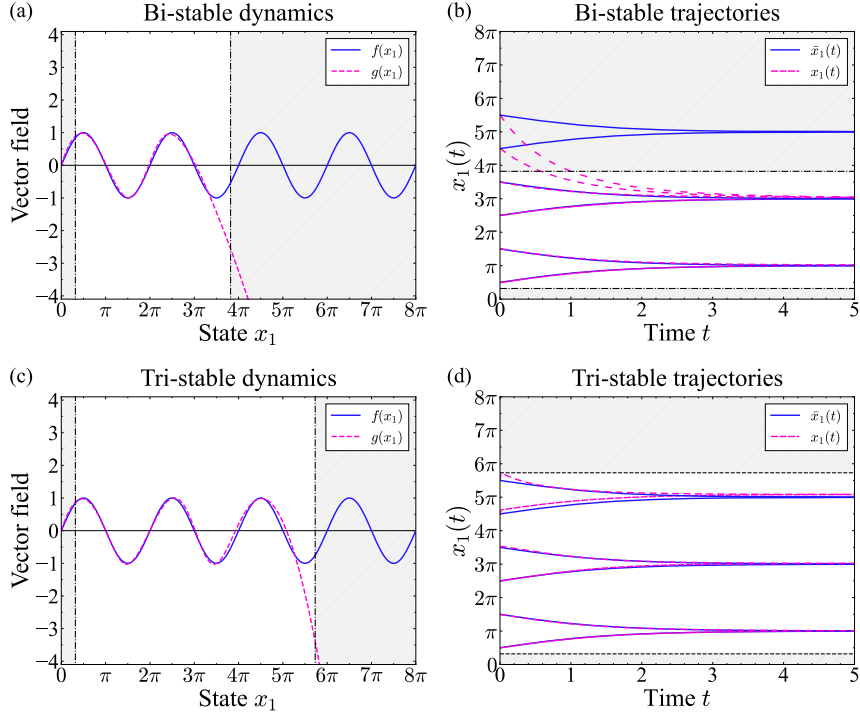


Figure 2: RNCRN approximations of the multi-stable target system (8). (a) The vector field of the target system (8) and reduced bi-stable system (9) when $\mathbb{K}_1 = [1, 12]$. (b) Solutions $\bar{x}_1(t)$ of the target system (8), and $x_1(t)$ of the full system (10) with $\mu = 0.01$. Analogous plots are shown in panels (c) and (d) for the tri-stable RNCRN over $\mathbb{K}_1 = [1, 18]$ presented in Appendix B.1, with reduced and full ODEs given respectively by (27) and (28), with coefficients (26) and $\mu = 0.01$. In panels (b) and (d), the initial concentrations of all chemical perceptrons are set to zero.

(b) *Dynamical approximation.* Let us apply the second step from Algorithm 1. Using the

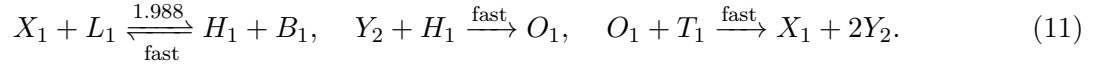
coefficients from (9), we now form the full ODEs (6):

$$\begin{aligned}
\frac{dx_1}{dt} &= -0.983x_1y_1 - 0.050x_1y_2 + 2.398x_1y_3, & x_1(0) &= a_1 \in \mathbb{K}_1, \\
\frac{dy_1}{dt} &= \frac{1}{\mu} + \frac{7.789}{\mu}y_1 - \frac{1.167}{\mu}x_1y_1 - \frac{1}{\mu}y_1^2, & y_1(0) &= b_1 \geq 0, \\
\frac{dy_2}{dt} &= \frac{1}{\mu} - \frac{1.918}{\mu}y_2 + \frac{0.994}{\mu}x_1y_2 - \frac{1}{\mu}y_2^2, & y_2(0) &= b_2 \geq 0, \\
\frac{dy_3}{dt} &= \frac{1}{\mu} + \frac{3.574}{\mu}y_3 - \frac{0.730}{\mu}x_1y_3 - \frac{1}{\mu}y_3^2, & y_3(0) &= b_3 \geq 0.
\end{aligned} \tag{10}$$

We fix the initial conditions arbitrarily to $b_1 = b_2 = b_3 = 0$, the desired final-time to $T = 5$ and the perceptron speed to $\mu = 0.01$. We then numerically integrate (8) and (10) over $t \in [0, 5]$ for a fixed initial concentration $a_1 \in \mathbb{K}_1$ of the executive species, and plot the solutions $\bar{x}(t)$ and $x(t)$; the same computations are then repeated for various values of a_1 , which we display in Figure 2(b). One can notice that the RNCRN underlying (10) with $\mu = 0.01$ accurately approximates the solutions of the target system; in particular, we observe bi-stability.

Tri-stability. One can similarly apply Algorithm 1 to (8) to obtain tri-stable RNCRNs. In particular, let us consider a larger set $\mathbb{K}_1 = [1, 18]$, which includes three stable equilibria, π , 3π , and 5π , and two unstable equilibria, 2π and 4π . Applying Algorithm 1, we find an RNCRN with $M = 4$ chemical perceptrons, which with $\mu = 0.01$ displays the desired tri-stability, as displayed in Figure 2(c)–(d); see Appendix B.1 for more details. In a similar manner, Algorithm 1 can be used to achieve RNCRNs with arbitrary number of stable equilibria; see Appendix B.1.

DNA-strand-displacement implementation. As outlined in Section 2.1, the RNCRN consists of abstract reactions, which must be appropriately enlarged for experimental implementations. As a demonstration, let us implement the RNCRN corresponding to the RREs (10) via an experimentally feasible DNA-strand-displacement system [62]. In this framework, e.g. the abstract reaction $X_1 + Y_2 \xrightarrow{1.988} X_1 + 2Y_2$, induced by the term $(0.994/\mu)x_1y_2$ with $\mu = 0.5$ from (10), is approximated with a system of 4 reactions involving 7 species, given by



Here, we denote the two irreversible reactions $X_1 + L_1 \xrightarrow{1.988} H_1 + B_1$ and $H_1 + B_1 \xrightarrow{\text{fast}} X_1 + L_1$ as a single reversible one; furthermore, some of the rate coefficients are described qualitatively as sufficiently “fast”, see Appendix C for more details. Species X_1 , Y_1 , B_1 and O_1 can be interpreted as suitable single-stranded DNA molecules, while L_1 , H_1 , T_1 as double-stranded DNA complexes; see Figure 3(a), where we display the DNA-based approximation (11) schematically.

In Appendix C, we approximate every reaction from the RNCRN induced by RREs (10) with a system of DNA-based reactions, such as (11); furthermore, we fix the perceptron speed to $\mu = 0.5$. For the resulting network, which we call the DNA-RNCRN, we assume that time and concentrations have units; furthermore, we rescale these quantities so that the concentrations of the DNA-species and rate coefficients fit within the physically admissible ranges [62]. By design, the DNA-RNCRN relies on suitable DNA species (e.g. L_1, B_1, T_1 from (11)) being present at sufficiently high concentrations. Being depleted over time, these fuel species must in general be replenished, e.g. by coupling the DNA-RNCRN to a chemostat [62]. In this paper, we do not model the replenishment process explicitly; instead, for simplicity, we assume that the fuel species are held constant. The resulting approximating *constant-fuel* RNCRN is given by (40) in Appendix C. In Figure 3(b), we display the concentration of the executive species from the constant-fuel DNA-RNCRN, demonstrating that

bistability is accurately replicated within experimentally feasible range. See Appendix C for more details, including a simulation of the DNA-RNCRN without the constant-fuel assumption.

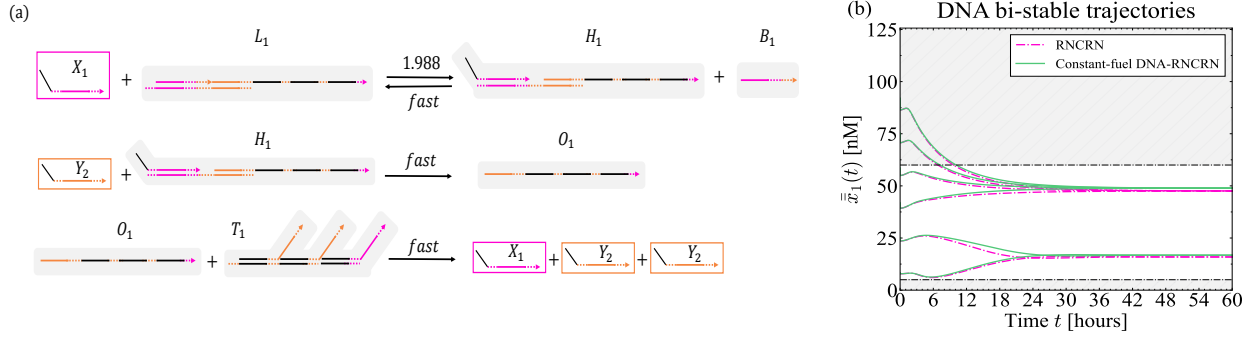


Figure 3: DNA-strand-displacement implementation of the RNCRN with RREs (10) with $\mu = 0.5$. (a) Domain-level representation of the DNA system (11), which approximates the bi-molecular reaction $X_1 + Y_2 \xrightarrow{1.988} X_1 + 2Y_2$. (b) Shown in purple is the concentrations $\bar{x}_1(t)$ of the executive species from a rescaled version of the RREs (10), given by (35) in Appendix C. Also shown in green is the corresponding concentration of the executive species from the constant-fuel RNCRN given by (40) in Appendix C. The concentrations are measured in nanomoles (nM), while time in hours.

4.2 Oscillations

Let us consider the two-variable target ODE system

$$\begin{aligned} \frac{d\bar{x}_1}{dt} &= f_1(\bar{x}_1, \bar{x}_2) = 6 + 4J_0\left(\frac{3}{2}\bar{x}_1\right) - \bar{x}_2, & \bar{x}_1(0) &= a_1 \geq 0, \\ \frac{d\bar{x}_2}{dt} &= f_2(\bar{x}_1, \bar{x}_2) = \bar{x}_1 - 4, & \bar{x}_2(0) &= a_2 \geq 0, \end{aligned} \quad (12)$$

were $J_0(\bar{x}_1)$ is the Bessel function of the first kind. Numerical simulations suggest that (12) has an isolated oscillatory solution, which we display as the blue curve in the (\bar{x}_1, \bar{x}_2) -space in Figure 4(a); also shown as grey arrows is the vector field, and as the unshaded box we display the desired region of interest $\mathbb{K}_1 \times \mathbb{K}_2 = [1, 8] \times [2, 10]$. In Figure 4(c), we show as solid blue curves this oscillatory solution in the (t, \bar{x}_1) - and (t, \bar{x}_2) -space.

Using Algorithm 1, we find an RNCRN with $M = 6$ chemical perceptrons, whose dynamics with $\mu = 0.01$ qualitatively matches that of the target system (12) within $\mathbb{K}_1 \times \mathbb{K}_2$; see Appendix B.2 for details. We display the solution of this RNCRN as the purple curve in Figure 4(b)–(c).

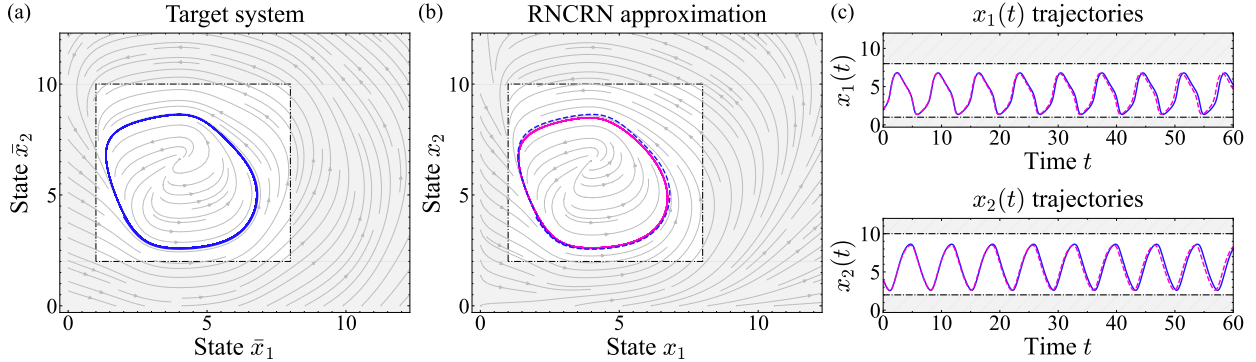


Figure 4: RNCRN approximation of the oscillatory target system (12). (a) The vector field of (12) is shown as grey arrows, the target region $\mathbb{K}_1 \times \mathbb{K}_2 = [1, 8] \times [2, 10]$ as the unshaded box, and the solution of (12) with $\bar{x}_1(0) = 2$ and $\bar{x}_2(0) = 4$ in blue. (b) Analogous plot is shown for the RNCRN from Appendix B.2, whose reduced and full ODEs are given respectively by (30) and (31), with coefficients (29) and $\mu = 0.01$. In particular, displayed as grey arrows is the vector field of the reduced ODEs (30), together with an oscillatory solution of the full ODEs (31) shown in purple; for comparison, we also display as dashed blue curve the oscillatory solution of (12). (c) Solutions $\bar{x}_1(t)$ and $x_1(t)$, and $\bar{x}_2(t)$ and $x_2(t)$. The initial concentrations of all perceptrons are fixed to zero.

Robustness. When implementing RNCRN, the underlying rate coefficients and initial conditions cannot be experimentally fine-tuned with perfect accuracy. Therefore, it is of great importance to study how the dynamics of RNCRN behaves under the parameter perturbations. A detailed analysis of this problem is beyond the scope of this paper. As a step forward, we numerically investigate sensitivity of the oscillatory solution of the RNCRN from Appendix B.2, which approximates the target system (12); see Appendix D for details. In particular, we perturb all the rate coefficients in the RNCRN by up to 50%, and compute the fraction of such perturbed RNCRN that qualitatively retain the periodic solution as a function of the perturbation noise. The results for the RNCRN with $\mu = 0.1$ are presented in Figure 5(a) in purple, with example trajectories in Figure 5(b); we observe that e.g. around 35% of systems still oscillate when the coefficients are perturbed by 10%. Also shown in Figure 5(a) in green are the results for the underlying quasi-static approximation, formally obtained by setting $\mu = 0$. One can notice that this approximation shows a similar degree of robustness, suggesting that the perceptron speed is not a major source of sensitivity. This observation is confirmed in Figure 5(c)–(d), which shows that the RNCRN is insensitive to a broad range of perturbations in μ . Robustness over a broad range of perturbations can also be observed with respect to the initial conditions, see Figure 5(e)–(f).

Noisy training. Figure 5 demonstrates that the RNCRN from Appendix B.2, while not being pathologically sensitive to the perturbations in the rate coefficients, is nevertheless much more vulnerable to such perturbations than those in perceptron speed and initial conditions. Let us now demonstrate that, by slightly modifying Algorithm 1, the rate-coefficient robustness can be significantly improved. In particular, step (a) of Algorithm 1 approximates the target vector field from (12) with the deterministic reduced vector field from (7). In Appendix D.4, we modify this step, by introducing suitable stochastic perturbations into the reduced vector field. We apply this noisy version of Algorithm 1 to design a new RNCRN, presented in Appendix D.4, which also contains $M = 6$ chemical perceptrons and approximates (12). This noise-trained RNCRN displays a significantly better robustness profile, as demonstrated in yellow in Figure 5(a); in particular, now almost all of the systems still oscillate when the rate coefficients are perturbed by 10%, and more

than 60% oscillate when the coefficients are perturbed by as much as 50%.

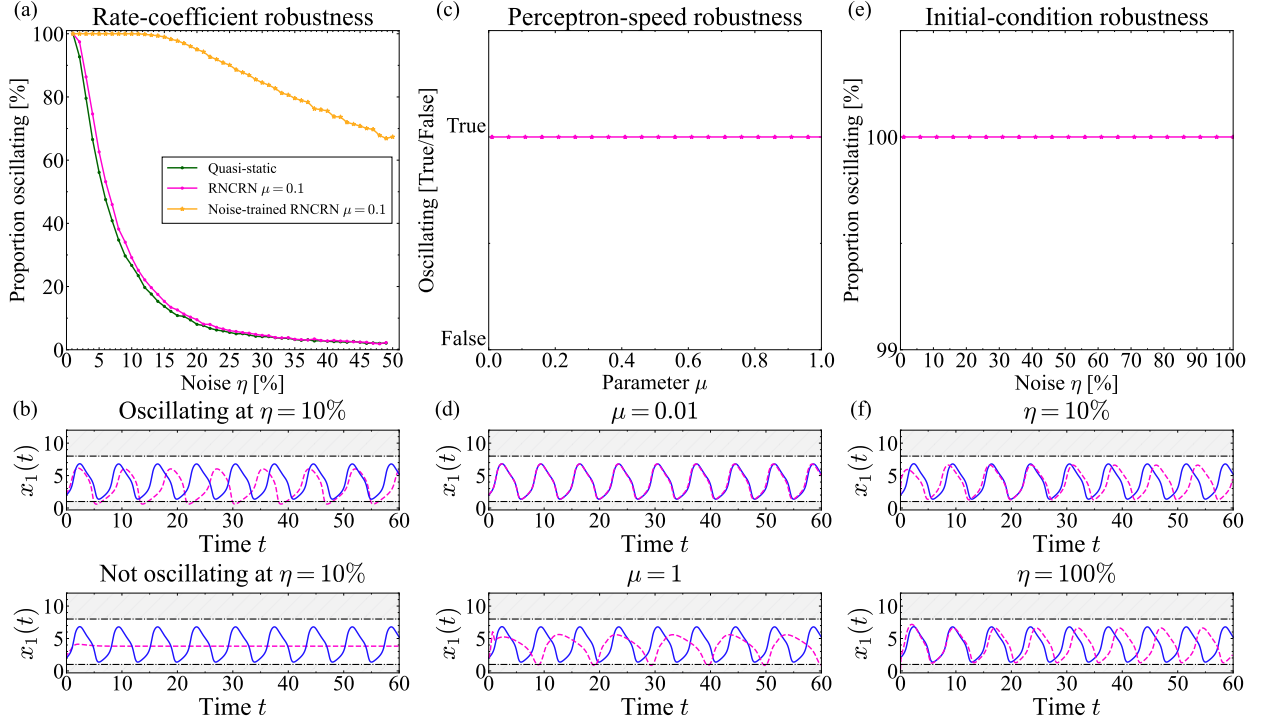


Figure 5: Robustness of RNCrNs approximating oscillatory target system (12). (a) Proportion of RNCrNs with perturbed rate coefficients that retain oscillations as a function of the perturbation noise. This proportion is shown in green for the quasi-static approximation (30), in purple for the corresponding RNCrN (31) with $\mu = 0.1$, and in yellow for the noise-trained RNCrN (46) with $\mu = 0.1$; see Appendix D.1 and D.4 for more details. Example trajectories of the RNCrN (31) which retain and do not retain oscillations are shown in purple in panel (b), together with the corresponding solutions of (12) in blue. (c) Preservation of oscillations in the RNCrN (31) as parameter μ is varied, with example trajectories shown in panel (d); see Appendix D.2 for more details. (e) Proportion of the RNCrNs (31) with perturbed initial conditions that retain oscillations, with example trajectories shown in panel (f); see Appendix D.3 for more details. Each point in panels (a), (c) and (e) was obtained by considering 10^4 independently perturbed RNCrNs.

4.3 Chaos

As our final example, we consider the three-variable target ODE system

$$\begin{aligned}
 \frac{d\bar{x}_1}{dt} &= f_1(\bar{x}_1, \bar{x}_2, \bar{x}_3) = 2.5\bar{x}_1(1 - 1.5\bar{x}_1) - \frac{4\bar{x}_1\bar{x}_2}{1 + 3\bar{x}_1}, & \bar{x}_1(0) &= 0.25, \\
 \frac{d\bar{x}_2}{dt} &= f_2(\bar{x}_1, \bar{x}_2, \bar{x}_3) = -0.4\bar{x}_2 + \frac{4\bar{x}_1\bar{x}_2}{1 + 3\bar{x}_1} - \frac{4\bar{x}_2\bar{x}_3}{1 + 3\bar{x}_2}, & \bar{x}_2(0) &= 0.25, \\
 \frac{d\bar{x}_3}{dt} &= f_3(\bar{x}_1, \bar{x}_2, \bar{x}_3) = -0.6\bar{x}_3 + \frac{4\bar{x}_2\bar{x}_3}{1 + 3\bar{x}_2}, & \bar{x}_3(0) &= 0.25.
 \end{aligned} \tag{13}$$

ODEs (13) are known as the Hasting-Powell system [66], and have been reported to exhibit chaotic behaviour. We present a portion of the state-space of (13) in Figure 6(a).

Using Algorithm 1, we find an RNCRN with $M = 5$ chemical perceptrons to approximate the dynamics of the Hasting-Powell system (13) over the compact set $x_1 \in \mathbb{K}_1$, $x_2 \in \mathbb{K}_2$ and $x_3 \in \mathbb{K}_3$ with $\mathbb{K}_1 = \mathbb{K}_2 = \mathbb{K}_3 = [0.01, 1]$. The parameters and the RREs can be found in Appendix B.3. The state-space for the executive species from the RNCRN is presented in Figure 6(b) when $\mu = 0.1$, suggesting presence of a chaotic attractor, in qualitative agreement with Figure 6(a). In Figure 6(c), we display the underlying time-trajectories. Let us note that alignment of the trajectories is not expected for long intervals of time due to the chaotic nature of the target system.

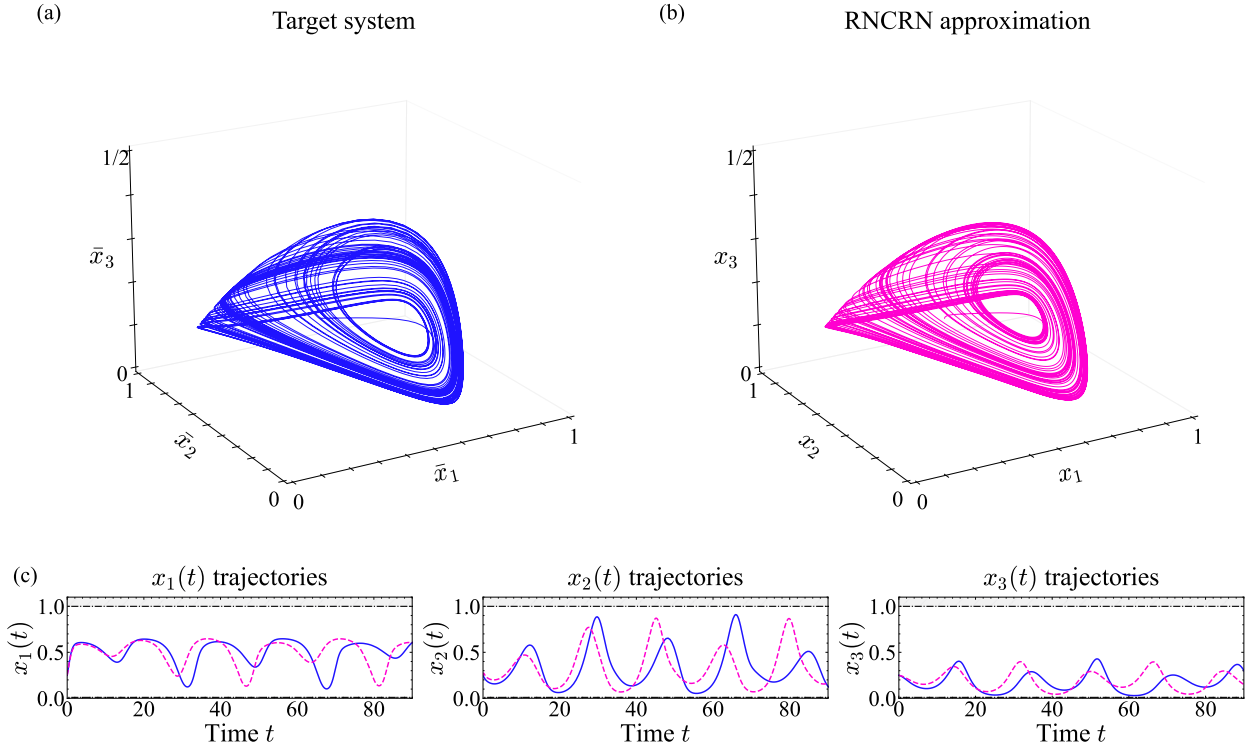


Figure 6: RNCRN approximation of the target system (13) with a chaotic attractor. (a) Solution of (13) in the state-space. (b) Solution of the RNCRN RREs (34) in the state-space, with coefficients (32), $\mu = 0.1$, initial conditions $x_1(0) = x_2(0) = x_3(0) = 0.25$, and zero initial conditions for all perceptrons. (c) Target and executive solutions $\bar{x}_i(t)$ and $x_i(t)$ for $i = 1, 2, 3$.

5 Discussion

In this paper, we have introduced a class of chemical reaction networks (CRNs) that can be trained to approximate the dynamics of any well-behaved system of ordinary-differential equations (ODEs). These recurrent neural chemical reaction networks (RNCRNs) operate by continually actuating the concentrations of the executive species such that they adhere to the target vector field which has been encoded by a faster system of chemical perceptrons. In Appendix A, we have proven the approximation abilities of RNCRNs. Based on this result, we have put forward Algorithm 1 for training RNCRNs, which relies on the backpropagation algorithm from the theory of artificial neural networks (ANNs). Due to the nature of backpropagation, Algorithm 1 is not guaranteed to find an optimal solution; nevertheless, it proved effective for the target systems presented in this paper. In particular, in Section 4, we showcased examples of RNCRNs that replicate sophisticated dynamical

behaviors with no more than six chemical perceptrons, governed by reactions which fire at most two orders of magnitude faster than those governing the executive species.

For target systems of ODEs with purely polynomial right-hand sides, there exist a number of other methods, which we call *chemical maps*, to design dynamically-equivalent CRNs [59,67–73]. CRNs designed using these chemical maps have analytically determined rate coefficients, i.e. they do not require numerical methods, such as the backpropagation algorithm, for this purpose; furthermore, these CRNs can involve less auxiliary species than RNCRNs. However, an advantage of RNCRNs is their ANN-based ability to replicate the dynamics of, not only ODEs with polynomial, but also non-polynomial right-hand sides, the latter of which can display a richer set of dynamical behaviors compared to the former. In Section 4, we have exploited this fact by considering example ODEs that contain a mixture of polynomial and non-polynomial terms. Let us also note that the structure of CRNs obtained via chemical maps depends on the given target ODE system. On the other hand, RNCRNs have a fixed structure, independent of the complexity of the target system, only relying on the reactions from Table 1; this modularity may be beneficial for experimentally building RNCRNs.

For target systems of ODEs with non-polynomial right-hand sides, there also exists an alternative scheme. In particular, under this scheme, one first maps the non-polynomial ODEs to polynomial ones [74], which is then followed by an application of a desired chemical map. Similar to RNCRNs, this scheme also introduces auxiliary variables to achieve the desired dynamics. However, in stark contrast to RNCRNs, owing to the map from [74], this alternative scheme displays a particular fragility: the initial conditions for the auxiliary species are constrained to particular values, and some deviations may cause some species concentrations to blow-up. In Appendix E, we demonstrate such chemically hazardous events when the scheme is applied to the target system (8). This fragility not only requires high-precision calibration of the initial conditions, but also effectively requires the preparation of an entirely different experiment for different executive species initial conditions. In contrast, no such adjustment of the auxiliary species is necessary for RNCRNs.

While certain properties of RNCRNs are experimentally desirable, such as modularity and robustness in initial concentrations of the auxiliary species (which form the bulk of initial conditions), there are several challenges present in chemistry that are not present in traditional electronic-based ANNs; in what follows, we focus on DNA-strand-displacement technologies [62]. Firstly, adding a perceptron or a new connection to an ANN is trivial compared to adding a chemical perceptron or a reaction to an RNCRN, which requires engineering a chemical species with specific reactivity. Secondly, compared to electronic circuits, chemical systems are much more prone to unintended interactions, so that the modularity of each chemical perceptron might break down as the network scales in size [18]. Finally, the weight parameters and inputs of an ANN can be fine-tuned to a high degree of precision. However, despite techniques to modulate the effective rates of chemical reactions, the calibration is significantly less precise than in electronic circuits [75,76], and the same is true for the initial conditions [50]. In this context, it is important to study how the dynamics of RNCRNs respond to perturbations in both the rate coefficients and all the initial conditions. In Section 4.2 and Appendix D, we have performed a preliminary study of this problem, showing favorable results; more detailed studies will form a part of future work. Let us also note that, in the light of the experimental challenges, we have focused in this paper on the single-layer (shallow) RNCRNs. In Appendix A, we have also presented multi-layer (deep) RNCRNs; in future work, we will study whether such deep RNCRNs have sufficiently advantageous approximation abilities to justify the additional experimental complexity.

Despite the various experimental challenges, DNA-strand-displacement technologies have been used to build intricate chemical systems of great complexity. In particular, under this framework, arbitrary bi-molecular CRNs, whose rate coefficients span up to six orders of magnitude [75], can

be implemented, and this approach has been used to build chemical systems with more than 100 species [35,36]. In Section 4.1 and Appendix C, we have implemented an RNCRN via DNA-strand-displacement under experimentally feasible conditions. In this context, a natural extension is the addition of enzymes, which can enhance the capabilities of the DNA circuits. For example, RNA polymerase has been used to continually produce strand displacement components [77,78], while strand-displacing polymerase [64] and the trio of polymerase, endonuclease and nickase (PEN) [42,52] can also be used to realize a range of chemical reactions. Such enzyme-based approaches have the potential to enable more universal, easily supplied fuel (in the form of nucleotide triphosphates) to maintain the concentrations of suitable auxiliary components for longer intervals of time, as well as to speed-up some of the underlying reactions.

We have used DNA strand-displacement to demonstrate experimental implementability of RNCRNs. More broadly, RNCRNs can be implemented with different physical media, provided the existence of a compilation framework from CRNs to such media [62–64]. Therefore, the results presented in this paper have the potential to generalize to other nanotechnological and synthetic biological contexts. In particular, given that RNCRNs contain slow and fast species, it is natural to consider architectures that operate over multiple time-scales. Important examples are transcription-factor networks. These networks have been shown to leverage the innate difference in the speed between the slow protein production and degradation, and the fast protein-protein interactions [56]; furthermore, the transcription-factor binding sites display dose thresholding reminiscent of a perceptron [79]. In this context, one can envisage the total concentration of each protein as the (slow) executive species concentration, and the concentrations of particular conformational states of the proteins as the (fast) chemical perceptron concentrations. Since the ODE models of transcription-factor networks have on the right-hand side rational functions, and not polynomials, the underlying activation function would be different from the one considered in this paper. Nevertheless, the results we present in Appendix A readily generalize to any non-polynomial activation function, allowing for construction of RNCRN-like networks based on transcription factors. Beyond chemistry and genetic circuits, RNCRNs may also find applications in immunology [80] and population dynamics [81]. In particular, let us note that the ODEs describing microbial cellular communities [82] are reminiscent of those governing chemical perceptrons presented in this paper.

6 Acknowledgements

Author Contributions: AD, BQ, TEO, and TP conceptualized the study; AD and TP performed the mathematical analyses; AD performed the numerical simulations and produced the figures; AD and TP wrote the paper; BQ and TEO reviewed the paper.

Funding: Alexander Dack acknowledges funding from the Department of Bioengineering at Imperial College London. Benjamin Qureshi was funded by the European Research Council (ERC) under the European Union’s Horizon 2020 research and innovation program (Grant agreement No. 851910). Thomas E. Ouldridge would like to thank the Royal Society for a University Research Fellowship. Tomislav Plesa would like to thank Peterhouse, University of Cambridge, for a Fellowship.

Declaration of interests: The authors declare no competing interests.

Acknowledgments: We thank Chris P. Barnes and Kathleen J. Y. Zhang for useful discussions about synthetic microbial communities.

Data and code availability: Data and code to be made available in a public repository with a DOI upon publication. During the review process you may access the following GitHub repository [83]: https://github.com/alexmack/recurrent_neural_chemical_reaction_networks.

References

- [1] W. S. McCulloch and W. Pitts, “A logical calculus of ideas immanent in nervous activity,” *Bulletin of Mathematical Biophysics*, vol. 5, pp. 115–133, 1943.
- [2] G. Cybenko, “Approximation by superpositions of a sigmoidal function,” *Mathematics of Control, Signals, and Systems*, vol. 2, pp. 303–314, 1989.
- [3] K. Hornik, M. Stinchcombe, and H. White, “Multilayer feedforward networks are universal approximators,” *Neural Networks*, vol. 2, pp. 359–366, 1989.
- [4] A. Pinkus, “Approximation theory of the MLP model in neural networks,” *Acta Numerica*, vol. 8, pp. 143–195, 1999.
- [5] Y. LeCun, Y. Bengio, and G. Hinton, “Deep learning,” *Nature*, vol. 521, pp. 436–444, 2015.
- [6] R. T. Q. Chen, Y. Rubanova, J. Bettencourt, and D. Duvenaud, “Neural Ordinary Differential Equations,” 2018.
- [7] J. J. Hopfield, “Neurons with graded response have collective computational properties like those of two-state neurons,” *Proceedings of the National Academy of Sciences*, vol. 81, pp. 3088–3092, May 1984.
- [8] D. Krotov and J. Hopfield, “Large Associative Memory Problem in Neurobiology and Machine Learning,” Apr. 2021. arXiv:2008.06996.
- [9] L. Perko, “Differential equations and dynamical systems,” *3rd Edition, Springer-Verlag*, 2001.
- [10] K.-i. Funahashi and Y. Nakamura, “Approximation of dynamical systems by continuous time recurrent neural networks,” *Neural Networks*, vol. 6, pp. 801–806, Jan. 1993.
- [11] J. Pathak, B. Hunt, M. Girvan, Z. Lu, and E. Ott, “Model-Free Prediction of Large Spatiotemporally Chaotic Systems from Data: A Reservoir Computing Approach,” *Physical Review Letters*, vol. 120, p. 024102, Jan. 2018.
- [12] M. Kimura and R. Nakano, “Learning dynamical systems by recurrent neural networks from orbits,” *Neural Networks*, vol. 11, pp. 1589–1599, Dec. 1998.
- [13] M.-a. Sato and Y. Murakami, “Learning nonlinear dynamics by recurrent neural networks (some problems on the theory of dynamical systems in applied sciences),” *数理解析研究所講究録*, vol. 760, pp. 71–87, 1991.
- [14] M. A. Bucci, O. Semeraro, A. Allauzen, G. Wisniewski, L. Cordier, and L. Mathelin, “Control of chaotic systems by deep reinforcement learning,” *Proceedings of the Royal Society A: Mathematical, Physical and Engineering Sciences*, vol. 475, p. 20190351, 2019.
- [15] L. Cardelli, M. Tribastone, and M. Tschaikowski, “From electric circuits to chemical networks,” *Natural Computing*, vol. 19, pp. 237–248, 2020.
- [16] A. Arkin and J. Ross, “Computational functions in biochemical reaction networks,” *Biophysical Journal*, vol. 67, pp. 560–578, 1994.
- [17] G. Seelig, D. Soloveichik, D. Y. Zhang, and E. Winfree, “Enzyme-Free Nucleic Acid Logic Circuits,” *Science*, vol. 314, pp. 1585–1588, 2006.

- [18] L. Qian and E. Winfree, “Scaling Up Digital Circuit Computation with DNA Strand Displacement Cascades,” *Science*, vol. 332, pp. 1196–1201, 2011.
- [19] D. Del Vecchio, A. J. Dy, and Y. Qian, “Control theory meets synthetic biology,” *Journal of The Royal Society Interface*, vol. 13, p. 20160380, 2016.
- [20] C. Briat, A. Gupta, and M. Khammash, “Antithetic Integral Feedback Ensures Robust Perfect Adaptation in Noisy Biomolecular Networks,” *Cell Systems*, vol. 2, pp. 15–26, 2016.
- [21] T. Plesa, G.-B. Stan, T. E. Ouldridge, and W. Bae, “Quasi-robust control of biochemical reaction networks via stochastic morphing,” *Journal of The Royal Society Interface*, vol. 18, p. 20200985, 2021.
- [22] M. Feinberg, “Lecture notes on chemical reaction networks,” *Lecture Notes, Mathematics Research Center, University of Wisconsin-Madison*, 1979.
- [23] A. Hjelmfelt, E. D. Weinberger, and J. Ross, “Chemical implementation of neural networks and Turing machines,” *Proceedings of the National Academy of Sciences*, vol. 88, pp. 10983–10987, 1991.
- [24] L. Qian, E. Winfree, and J. Bruck, “Neural network computation with DNA strand displacement cascades,” *Nature*, vol. 475, pp. 368–372, 2011.
- [25] J. Kim, J. Hopfield, and E. Winfree, “Neural Network Computation by In Vitro Transcriptional Circuits,” *Advances in Neural Information Processing Systems*, vol. 17, 2004.
- [26] H.-J. K. Chiang, J.-H. R. Jiang, and F. Fages, “Reconfigurable neuromorphic computation in biochemical systems,” in *2015 37th Annual International Conference of the IEEE Engineering in Medicine and Biology Society (EMBC)*, pp. 937–940, 2015.
- [27] M. Vasić, C. Chalk, A. Luchsinger, S. Khurshid, and D. Soloveichik, “Programming and training rate-independent chemical reaction networks,” *Proceedings of the National Academy of Sciences*, vol. 119, p. e2111552119, 2022.
- [28] J. Linder, Y.-J. Chen, D. Wong, G. Seelig, L. Ceze, and K. Strauss, “Robust Digital Molecular Design of Binarized Neural Networks,” in *27th International Conference on DNA Computing and Molecular Programming (DNA 27)*, vol. 205, pp. 1:1–1:20, 2021.
- [29] D. F. Anderson, B. Joshi, and A. Deshpande, “On reaction network implementations of neural networks,” *Journal of The Royal Society Interface*, vol. 18, p. 20210031, 2021.
- [30] R. T. Nagipogu and J. H. Reif, “NeuralCRNs: A Natural Implementation of Learning in Chemical Reaction Networks,” Aug. 2024. arXiv:2409.00034.
- [31] C. Kieffer, A. J. Genot, Y. Rondelez, and G. Gines, “Molecular Computation for Molecular Classification,” *Advanced Biology*, vol. 7, p. 2200203, 2023.
- [32] C. C. Samaniego, E. Wallace, F. Blanchini, E. Franco, and G. Giordano, “Neural networks built from enzymatic reactions can operate as linear and nonlinear classifiers,” *bioRxiv*, 2024.
- [33] A. J. Van Der Linden, P. A. Pieters, M. W. Bartelds, B. L. Nathalia, P. Yin, W. T. S. Huck, J. Kim, and T. F. A. De Greef, “DNA Input Classification by a Riboregulator-Based Cell-Free Perceptron,” *ACS Synthetic Biology*, vol. 11, pp. 1510–1520, 2022.

- [34] W. Poole, A. Ortiz-Muñoz, A. Behera, N. S. Jones, T. E. Ouldridge, E. Winfree, and M. Gopalkrishnan, “Chemical Boltzmann Machines,” in *DNA 2017: DNA Computing and Molecular Programming*, vol. 10467, pp. 210–231, 2017.
- [35] K. M. Cherry and L. Qian, “Scaling up molecular pattern recognition with DNA-based winner-take-all neural networks,” *Nature*, vol. 559, pp. 370–376, 2018.
- [36] X. Xiong, T. Zhu, Y. Zhu, M. Cao, J. Xiao, L. Li, F. Wang, C. Fan, and H. Pei, “Molecular convolutional neural networks with DNA regulatory circuits,” *Nature Machine Intelligence*, vol. 4, pp. 625–635, 2022.
- [37] A. Moorman, C. C. Samaniego, C. Maley, and R. Weiss, “A Dynamical Biomolecular Neural Network,” in *2019 IEEE 58th Conference on Decision and Control (CDC)*, pp. 1797–1802, 2019. ISSN: 2576-2370.
- [38] R. Lopez, R. Wang, and G. Seelig, “A molecular multi-gene classifier for disease diagnostics,” *Nature Chemistry*, vol. 10, pp. 746–754, 2018.
- [39] A. J. Genot, T. Fujii, and Y. Rondelez, “Scaling down DNA circuits with competitive neural networks,” *Journal of The Royal Society Interface*, vol. 10, p. 20130212, 2013.
- [40] A. Pandi, M. Koch, P. L. Voyvodic, P. Soudier, J. Bonnet, M. Kushwaha, and J.-L. Faulon, “Metabolic perceptrons for neural computing in biological systems,” *Nature Communications*, vol. 10, p. 3880, 2019.
- [41] X. Li, L. Rizik, V. Kravchik, M. Khoury, N. Korin, and R. Daniel, “Synthetic neural-like computing in microbial consortia for pattern recognition,” *Nature Communications*, vol. 12, p. 3139, 2021.
- [42] S. Okumura, G. Gines, N. Lobato-Dauzier, A. Baccouche, R. Deteix, T. Fujii, Y. Rondelez, and A. J. Genot, “Nonlinear decision-making with enzymatic neural networks,” *Nature*, vol. 610, pp. 496–501, 2022.
- [43] F. Rosenblatt, *The perceptron, a perceiving and recognizing automaton Project Para*. Cornell Aeronautical Laboratory, 1957.
- [44] G. Tkačik and P. R. T. Wolde, “Information Processing in Biochemical Networks,” *Annual Review of Biophysics*, Feb. 2025.
- [45] W. Xiong and J. E. Ferrell, “A positive-feedback-based bistable ‘memory module’ that governs a cell fate decision,” *Nature*, vol. 426, pp. 460–465, Nov. 2003.
- [46] P. E. Hardin, J. C. Hall, and M. Rosbash, “Feedback of the *Drosophila* period gene product on circadian cycling of its messenger RNA levels,” *Nature*, vol. 343, pp. 536–540, Feb. 1990.
- [47] R. Lev Bar-Or, R. Maya, L. A. Segel, U. Alon, A. J. Levine, and M. Oren, “Generation of oscillations by the p53-Mdm2 feedback loop: A theoretical and experimental study,” *Proceedings of the National Academy of Sciences*, vol. 97, pp. 11250–11255, Oct. 2000.
- [48] M. L. Heltberg, S. Krishna, and M. H. Jensen, “On chaotic dynamics in transcription factors and the associated effects in differential gene regulation,” *Nature Communications*, vol. 10, p. 71, Jan. 2019.

- [49] D. Choudhary, K. R. Foster, and S. Uphoff, “Chaos in a bacterial stress response,” *Current Biology*, vol. 33, pp. 5404–5414.e9, Dec. 2023.
- [50] N. Srinivas, J. Parkin, G. Seelig, E. Winfree, and D. Soloveichik, “Enzyme-free nucleic acid dynamical systems,” *Science*, vol. 358, p. eaal2052, Dec. 2017.
- [51] A. P. Lapteva, N. Sarraf, and L. Qian, “DNA Strand-Displacement Temporal Logic Circuits,” *Journal of the American Chemical Society*, vol. 144, pp. 12443–12449, July 2022.
- [52] T. Fujii and Y. Rondelez, “Predator–Prey Molecular Ecosystems,” *ACS Nano*, vol. 7, pp. 27–34, Jan. 2013.
- [53] J. Y. Kishi, T. E. Schaus, N. Gopalkrishnan, F. Xuan, and P. Yin, “Programmable autonomous synthesis of single-stranded DNA,” *Nature Chemistry*, vol. 10, pp. 155–164, Feb. 2018.
- [54] N. Lobato-Dauzier, A. Baccouche, G. Gines, T. Levi, Y. Rondelez, T. Fujii, S. H. Kim, N. Aubert-Kato, and A. J. Genot, “Neural coding of temperature with a DNA-based spiking chemical neuron,” *Nature Chemical Engineering*, vol. 1, pp. 510–521, Aug. 2024.
- [55] J. Stricker, S. Cookson, M. R. Bennett, W. H. Mather, L. S. Tsimring, and J. Hasty, “A fast, robust and tunable synthetic gene oscillator,” *Nature*, vol. 456, pp. 516–519, Nov. 2008.
- [56] R. Zhu, J. M. Del Rio-Salgado, J. Garcia-Ojalvo, and M. B. Elowitz, “Synthetic multistability in mammalian cells,” *Science*, vol. 375, p. eabg9765, Jan. 2022.
- [57] A. Goudarzi, M. R. Lakin, and D. Stefanovic, “DNA Reservoir Computing: A Novel Molecular Computing Approach,” in *DNA Computing and Molecular Programming* (D. Soloveichik and B. Yurke, eds.), vol. 8141, pp. 76–89, Cham: Springer International Publishing, 2013.
- [58] M. G. Baltussen, T. J. De Jong, Q. Duez, W. E. Robinson, and W. T. S. Huck, “Chemical reservoir computation in a self-organizing reaction network,” *Nature*, vol. 631, pp. 549–555, July 2024.
- [59] T. Plesa, T. Vejchodský, and R. Erban, “Chemical reaction systems with a homoclinic bifurcation: an inverse problem,” *Journal of Mathematical Chemistry*, vol. 54, pp. 1884–1915, 2016.
- [60] T. Wilhelm, “Chemical systems consisting only of elementary steps – a paradigm for nonlinear behavior,” *Journal of Mathematical Chemistry*, vol. 27, pp. 71–88, 2000.
- [61] T. Plesa, “Stochastic approximations of higher-molecular by bi-molecular reactions,” *Journal of Mathematical Biology*, vol. 86, p. 28, 2023.
- [62] D. Soloveichik, G. Seelig, and E. Winfree, “DNA as a universal substrate for chemical kinetics,” *Proceedings of the National Academy of Sciences*, vol. 107, pp. 5393–5398, 2010.
- [63] Y.-J. Chen, N. Dalchau, N. Srinivas, A. Phillips, L. Cardelli, D. Soloveichik, and G. Seelig, “Programmable chemical controllers made from DNA,” *Nature Nanotechnology*, vol. 8, pp. 755–762, Oct. 2013.
- [64] S. Shah, T. Song, X. Song, M. Yang, and J. Reif, “Implementing Arbitrary CRNs Using Strand Displacing Polymerase,” in *DNA Computing and Molecular Programming* (C. Thachuk and Y. Liu, eds.), vol. 11648, pp. 21–36, Cham: Springer International Publishing, 2019.

- [65] D. E. Rumelhart, G. E. Hinton, and R. J. Williams, “Learning representations by back-propagating errors,” *Nature*, vol. 323, pp. 533–536, Oct. 1986.
- [66] L. Stone and D. He, “Chaotic oscillations and cycles in multi-trophic ecological systems,” *Journal of Theoretical Biology*, vol. 248, pp. 382–390, 2007.
- [67] T. Plesa, “Mapping dynamical systems into chemical reactions,” *Available as <https://arxiv.org/pdf/2406.03473>*, 2025.
- [68] N. Samardzija, L. D. Greller, and E. Wasserman, “Nonlinear chemical kinetic schemes derived from mechanical and electrical dynamical systems,” *The Journal of Chemical Physics*, vol. 90, pp. 2296–2304, 1989.
- [69] D. Poland, “Cooperative catalysis and chemical chaos: a chemical model for the Lorenz equations,” *Physica D: Nonlinear Phenomena*, vol. 65, pp. 86–99, 1993.
- [70] T. Plesa, T. Vejchodský, and R. Erban, “Test Models for Statistical Inference: Two-Dimensional Reaction Systems Displaying Limit Cycle Bifurcations and Bistability,” in *Stochastic Processes, Multiscale Modeling, and Numerical Methods for Computational Cellular Biology*, pp. 3–27, 2017.
- [71] T. Plesa, A. Dack, and T. E. Ouldridge, “Integral feedback in synthetic biology: Negative-equilibrium catastrophe (Appendix D),” *Journal of Mathematical Chemistry*, vol. 61, pp. 1980–2018, 2023.
- [72] K. M. Hantos and G. Szederkényi, “Mass action realizations of reaction kinetic system models on various time scales,” *Journal of Physics: Conference Series*, vol. 268, p. 012009, 2011.
- [73] K. Kowalski, “Universal formats for nonlinear dynamical systems,” *Chemical Physics Letters*, vol. 209, pp. 167–170, 1993.
- [74] E. H. Kerner, “Universal formats for nonlinear ordinary differential systems,” *Journal of Mathematical Physics*, vol. 22, pp. 1366–1371, 1981.
- [75] D. Y. Zhang and E. Winfree, “Control of dna strand displacement kinetics using toehold exchange,” *Journal of the American Chemical Society*, vol. 131, no. 47, pp. 17303–17314, 2009. PMID: 19894722.
- [76] N. E. C. Haley, T. E. Ouldridge, I. Mullor Ruiz, A. Geraldini, A. A. Louis, J. Bath, and A. J. Turberfield, “Design of hidden thermodynamic driving for non-equilibrium systems via mismatch elimination during DNA strand displacement,” *Nature Communications*, vol. 11, p. 2562, May 2020.
- [77] W. Bae, G.-B. V. Stan, and T. E. Ouldridge, “*In situ* Generation of RNA Complexes for Synthetic Molecular Strand-Displacement Circuits in Autonomous Systems,” *Nano Letters*, vol. 21, pp. 265–271, Jan. 2021.
- [78] S. W. Schaffter and E. A. Strychalski, “Cotranscriptionally encoded RNA strand displacement circuits,” *Science Advances*, vol. 8, p. eabl4354, Mar. 2022.
- [79] M. Spivakov, “Spurious transcription factor binding: Non-functional or genetically redundant?,” *BioEssays*, vol. 36, pp. 798–806, Aug. 2014.

- [80] J. Farmer, N. H. Packard, and A. S. Perelson, “The immune system, adaptation, and machine learning,” *Physica D: Nonlinear Phenomena*, vol. 22, pp. 187–204, Oct. 1986.
- [81] M. Hirafuji, K. Tanaka, and S. Hagan, “Lotka-Volterra machine for a general model of complex biological systems,” in *Proceedings of the 1999 IEEE International Symposium on Computer Aided Control System Design (Cat. No.99TH8404)*, (Kohala Coast, HI, USA), pp. 516–521, IEEE, 1999.
- [82] R. R. Stein, V. Bucci, N. C. Toussaint, C. G. Buffie, G. Rättsch, E. G. Pamer, C. Sander, and J. B. Xavier, “Ecological Modeling from Time-Series Inference: Insight into Dynamics and Stability of Intestinal Microbiota,” *PLOS Computational Biology*, vol. 9, p. e1003388, Dec. 2013.
- [83] A. Dack, B. Qureshi, T. E. Ouldridge, and T. Plesa, “github.com/alexduck/recurrent_neural_chemical_reaction_networks,” Jul 2024.
- [84] E. A. Coddington and N. Levinson, *Theory of Ordinary Differential Equations*. New-York: McGraw-Hill, 1995.
- [85] W. Klonowski, “Simplifying principles for chemical and enzyme reaction kinetics,” *Biophysical Chemistry*, vol. 18, pp. 73–87, 1983.
- [86] A. N. Tikhonov, “Systems of differential equations containing small parameters in the derivatives,” *Mat. Sb. (N.S.)*, vol. 31(73), pp. 575–586, 1952.
- [87] D. Scalise, N. Dutta, and R. Schulman, “DNA Strand Buffers,” *Journal of the American Chemical Society*, vol. 140, pp. 12069–12076, Sept. 2018.

A Appendix: Universal approximation theorem for RNCRNs

In this section, we present the main theoretical result for single- and multi-layer RNCRNs.

A.1 Single-layer RNCRN

Consider the single-layer RNCRN given by

$$\begin{aligned} \emptyset &\xrightarrow{\beta_i} X_i, & X_i + Y_j &\xrightarrow{|\alpha_{i,j}|} X_i + \text{sign}(\alpha_{i,j})X_i + Y_j, \\ \emptyset &\xrightarrow{\gamma/\mu} Y_j, & Y_j &\xrightarrow{|\theta_j|/\mu} Y_j + \text{sign}(\theta_j)Y_j, & X_i + Y_j &\xrightarrow{|\omega_{j,i}|/\mu} X_i + Y_j + \text{sign}(\omega_{j,i})Y_j, & 2Y_j &\xrightarrow{1/\mu} Y_j, \end{aligned} \quad (14)$$

for $i = 1, 2, \dots, N$ and $j = 1, 2, \dots, M$, where for any real number $x \in \mathbb{R}$, we define $\text{sign}(x) = -1$ if $x < 0$, $\text{sign}(x) = 0$ if $x = 0$ and $\text{sign}(x) = 1$ if $x > 0$. The RREs induced by (14) are given by (6).

In what follows, we define $\mathbf{x} = (x_1, x_2, \dots, x_N) \in \mathbb{R}^N$, and collect all the rate coefficients $\alpha_{i,j}$, $\omega_{j,k}$, θ_j into suitable vectors $\boldsymbol{\alpha} \in \mathbb{R}^{NM}$, $\boldsymbol{\omega} \in \mathbb{R}^{MN}$, $\boldsymbol{\theta} \in \mathbb{R}^M$, respectively; similarly, we let $\boldsymbol{\beta} = (\beta_1, \beta_2, \dots, \beta_N) \in \mathbb{R}_{\geq}^N$. Furthermore, we define the *reduced vector field* by

$$g_i(\mathbf{x}) = g_i(\mathbf{x}; \boldsymbol{\alpha}, \boldsymbol{\beta}, \gamma, \boldsymbol{\omega}, \boldsymbol{\theta}) = \beta_i + x_i \sum_{j=1}^M \alpha_{i,j} \sigma_\gamma \left(\sum_{k=1}^N \omega_{j,k} x_k + \theta_j \right), \quad \text{for } i = 1, 2, \dots, N, \quad (15)$$

which appears on the right-hand side of (7).

Theorem A.1. (Universal approximation theorem for single-layer RNCNRNs) Consider the target ODE system (5) on a compact set $\mathbb{K} = \mathbb{K}_1 \times \mathbb{K}_2 \times \dots \times \mathbb{K}_N \subset \mathbb{R}_{\geq}^N$ in the state-space, with vector field (f_1, f_2, \dots, f_N) Lipschitz-continuous on \mathbb{K} . Consider also the single-layer RNCNRN (14) with RREs (6) with rate coefficients $\boldsymbol{\beta} = \boldsymbol{\beta}^* \in \mathbb{R}_{\geq}^N$ and $\gamma = \gamma^* > 0$ fixed to any values.

- (i) **Quasi-static approximation.** Consider the reduced vector field (15). Let $\varepsilon > 0$ be any given tolerance. Then, for every sufficiently large $M > 0$ there exist $\boldsymbol{\alpha}^* \in \mathbb{R}^{NM}$, $\boldsymbol{\omega}^* \in \mathbb{R}^{MN}$, and $\boldsymbol{\theta}^* \in \mathbb{R}^M$ such that

$$\max_{\mathbf{x} \in \mathbb{K}} |g_i(\mathbf{x}; \boldsymbol{\alpha}^*, \boldsymbol{\beta}^*, \gamma^*, \boldsymbol{\omega}^*, \boldsymbol{\theta}^*) - f_i(\mathbf{x})| \leq \varepsilon \text{ for all } i = 1, 2, \dots, N. \quad (16)$$

- (ii) **Dynamical approximation.** Assume that the solution of (5) exists for all $t \in [0, T]$ for some $T > 0$, and that $\bar{x}_i(t) \in \mathbb{K}_i$ for all $t \in [0, T]$ for all $i = 1, 2, \dots, N$. Then, for every sufficiently small $\varepsilon = \varepsilon^* > 0$ fixed there exists $\mu_0 > 0$ such that for all $\mu \in (0, \mu_0)$ system (6) has a unique solution $x_i(t) \in \mathbb{K}_i$ for all $t \in [0, T]$ for all $i = 1, 2, \dots, N$, and

$$\max_{t \in [0, T]} |x_i(t; \boldsymbol{\alpha}^*, \boldsymbol{\beta}^*, \gamma^*, \boldsymbol{\omega}^*, \boldsymbol{\theta}^*, \mu) - \bar{x}_i(t)| \leq c_1 \varepsilon^* + c_2 \mu \text{ for all } i = 1, 2, \dots, N, \quad (17)$$

where constants c_1 and c_2 are independent of μ .

Proof.

- (i) **Quasi-static approximation.** Consider continuous function $h_i : \mathbb{K} \rightarrow \mathbb{R}$ defined by $h_i(\mathbf{x}) = (f_i(\mathbf{x}) - \beta_i^*)/x_i$. Since the activation function σ_γ , defined by (4), is continuous and non-polynomial, it follows from [4][Theorem 3.1] that for any $\varepsilon > 0$ there exist $M > 0$, coefficients $\alpha_{i,j}^*, \omega_{j,k}^*, \theta_j^* \in \mathbb{R}$ and a continuous function $\rho_i(\mathbf{x})$ such that

$$h_i(\mathbf{x}) = \sum_{j=1}^M \alpha_{i,j}^* \sigma_{\gamma^*} \left(\sum_{k=1}^N \omega_{j,k}^* x_k + \theta_j^* \right) + \rho_i(\mathbf{x}) \text{ for all } i = 1, 2, \dots, N, \quad (18)$$

and $\max_{\mathbf{x} \in \mathbb{K}} |\rho_i(\mathbf{x})| \leq \varepsilon/X_i$, with $X_i = \max_{x_i \in \mathbb{K}_i} x_i$. Equation (18) implies (16).

- (ii) **Dynamical approximation.** It follows from (16) and regular perturbation theory [84] that there exists $\varepsilon_0 > 0$ such that for all $\varepsilon \in (0, \varepsilon_0)$

$$\max_{t \in [0, T]} |\tilde{x}_i(t; \boldsymbol{\alpha}^*, \boldsymbol{\beta}^*, \gamma^*, \boldsymbol{\omega}^*, \boldsymbol{\theta}^*) - \bar{x}_i(t)| \leq c_1 \varepsilon \text{ for all } i = 1, 2, \dots, N, \quad (19)$$

for some ε -independent constant $c_1 > 0$, where $\tilde{x}_i(t) = \tilde{x}_i(t; \boldsymbol{\alpha}^*, \boldsymbol{\beta}^*, \gamma^*, \boldsymbol{\omega}^*, \boldsymbol{\theta}^*)$ satisfies the reduced system (7). In what follows, we fix $\varepsilon = \varepsilon^* \in (0, \varepsilon_0)$.

Consider the fast (adjointed) system from (6), defined by

$$\frac{dy_j}{d\tau} = \gamma^* + \theta_j^* y_j + \left(\sum_{i=1}^N \omega_{j,i}^* x_i \right) y_j - y_j^2, \quad y_j(0) = b_j, \quad \text{for } j = 1, 2, \dots, M, \quad (20)$$

where x_1, x_2, \dots, x_N are parameters. The ODEs from (20) are decoupled, and each one has a unique non-negative continuously differentiable equilibrium $y_j = \sigma_{\gamma^*} \left(\sum_{k=1}^N \omega_{j,k}^* x_k + \theta_j^* \right)$, which is stable for all non-negative initial conditions $b_j \geq 0$. It follows from singular perturbation theory (Tikhonov's

theorem) [85, 86] that there exists $\mu_0 > 0$ such that for all $\mu \in (0, \mu_0)$ system (6) has a unique solution in \mathbb{K} over time-interval $[0, T]$, and

$$\max_{t \in [0, T]} |x_i(t; \boldsymbol{\alpha}^*, \boldsymbol{\beta}^*, \gamma^*, \boldsymbol{\omega}^*, \boldsymbol{\theta}^*, \mu) - \tilde{x}_i(t; \boldsymbol{\alpha}^*, \boldsymbol{\beta}^*, \gamma^*, \boldsymbol{\omega}^*, \boldsymbol{\theta}^*)| \leq c_2 \mu \text{ for all } i = 1, 2, \dots, N, \quad (21)$$

for some μ -independent constant $c_2 > 0$. Using $|x_i - \bar{x}_i| \leq |x_i - \tilde{x}_i| + |\tilde{x}_i - \bar{x}_i|$ and (19) and (21), one obtains (17). \square

Remark. In Theorem A.1, L_∞ -norm is used to measure the distance between the target and reduced vector fields. On the other hand, in Algorithm 1, we instead use the L_2 -norm, for computational simplicity. Rigorous justification of using the L_2 -norm is beyond the scope of this paper.

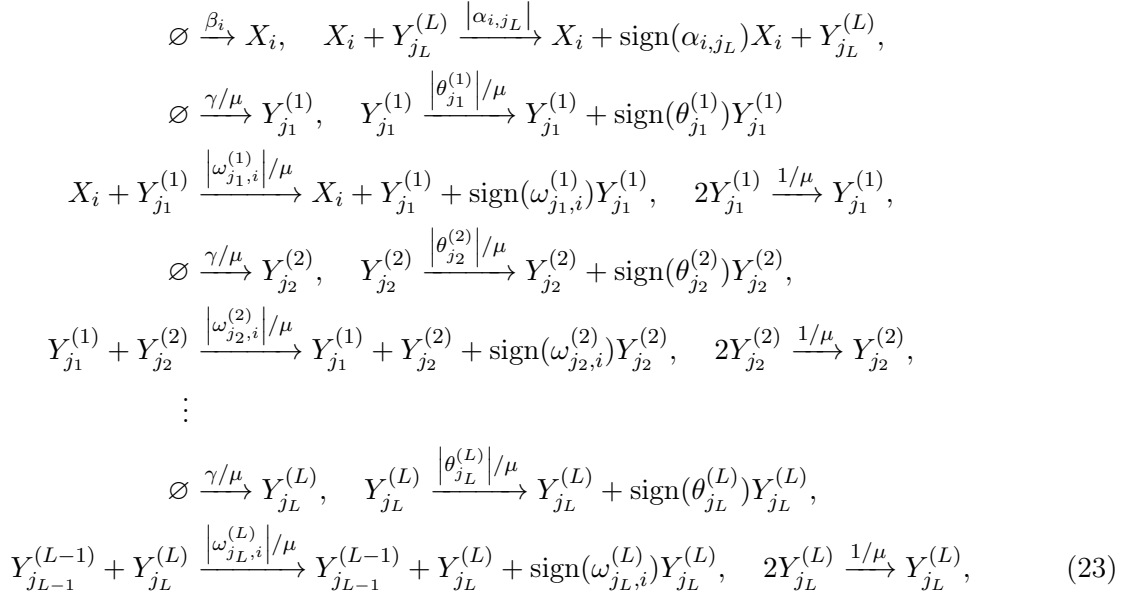
A.2 Multi-layer RNCRN

In the ANN context, *deep* neural networks, i.e. those containing multiple layer of neurons, are important [5]. In the CRN context, generalizing the single-layer RREs (6) to multi-layer ones yields

$$\begin{aligned} \frac{dx_i}{dt} &= \beta_i + x_i \sum_{k=1}^{M_L} \alpha_{i,k} y_k^{(L)}, & x_i(0) &= a_i, & \text{for } i = 1, 2, \dots, N, \\ \frac{dy_{j_1}^{(1)}}{dt} &= \frac{\gamma}{\mu} + \frac{\theta_j^{(1)}}{\mu} y_{j_1}^{(1)} + \left(\sum_{i=1}^N \frac{\omega_{j,i}^{(1)}}{\mu} x_i \right) y_{j_1}^{(1)} - \frac{1}{\mu} \left(y_{j_1}^{(1)} \right)^2, & y_{j_1}^{(1)}(0) &= b_{j_1} \geq 0, & \text{for } j_1 = 1, 2, \dots, M_1, \\ \frac{dy_{j_2}^{(2)}}{dt} &= \frac{\gamma}{\mu} + \frac{\theta_j^{(2)}}{\mu} y_{j_2}^{(2)} + \left(\sum_{k=1}^{M_1} \frac{\omega_{j,k}^{(2)}}{\mu} y_k^{(1)} \right) y_{j_2}^{(2)} - \frac{1}{\mu} \left(y_{j_2}^{(2)} \right)^2, & y_{j_2}^{(2)}(0) &= b_{j_2} \geq 0, & \text{for } j_2 = 1, 2, \dots, M_2, \\ &\vdots & & & \\ \frac{dy_{j_L}^{(L)}}{dt} &= \frac{\gamma}{\mu} + \frac{\theta_j^{(L)}}{\mu} y_{j_L}^{(L)} + \left(\sum_{k=1}^{M_{L-1}} \frac{\omega_{j,k}^{(L)}}{\mu} y_k^{(L-1)} \right) y_{j_L}^{(L)} - \frac{1}{\mu} \left(y_{j_L}^{(L)} \right)^2, & y_{j_L}^{(L)}(0) &= b_{j_L} \geq 0, & \text{for } j_L = 1, 2, \dots, M_L. \end{aligned} \quad (22)$$

In particular, (22) involves N executive species X_1, X_2, \dots, X_N , and L layers of chemical perceptrons, with the i th layer containing M_i perceptrons. In this hierarchy, the executive species X_1, X_2, \dots, X_N are inputs to the first layer of neurons $Y_1^{(1)}, \dots, Y_{M_1}^{(1)}$, which themselves are inputs to the second layer of neurons $Y_1^{(2)}, \dots, Y_{M_2}^{(2)}$, etc.; the final, L th, layer of neurons $Y_1^{(L)}, \dots, Y_{M_L}^{(L)}$ feeds back into

the executive species. The multi-layer RNCRN induced by (22) is given by



for $i = 1, \dots, N$ and $j_l = 1, \dots, M_l$.

Reduced ODEs. Multiplying the RREs of the chemical perceptrons from (22) by μ , and then fixing $\mu = 0$, it follows that their concentrations are given in the quasi-state state by

$$\begin{aligned}
(y_{j_1}^{(1)})^* &= \frac{1}{2} \left(\left(\sum_{i=1}^N \omega_{j_1,i}^{(1)} x_i + \theta_{j_1}^{(1)} \right) + \sqrt{\left(\sum_{i=1}^N \omega_{j_1,i}^{(1)} x_i + \theta_{j_1}^{(1)} \right)^2 + 4\gamma} \right), \\
&\vdots \\
(y_{j_L}^{(L)})^* &= \frac{1}{2} \left(\left(\sum_{k=1}^{M_{L-1}} \omega_{j_L,k}^{(L)} (y_k^{(L-1)})^* + \theta_{j_L}^{(L)} \right) + \sqrt{\left(\sum_{k=1}^{M_{L-1}} \omega_{j_L,k}^{(L)} (y_k^{(L-1)})^* + \theta_{j_L}^{(L)} \right)^2 + 4\gamma} \right), \tag{24}
\end{aligned}$$

for $j_l = 1, 2, \dots, M_l$. In this case, the executive species satisfy the reduced ODEs

$$\frac{dx_i}{dt} = g_i(x_1, \dots, x_N) = \beta_i + x_i \sum_{k=1}^{M_L} \alpha_{i,k} (y_k^{(L)})^*, \quad x_i(0) = a_i \geq 0, \quad \text{for } i = 1, 2, \dots, N. \tag{25}$$

One can formulate analogous theorem to Theorem A.1 for the multi-layer RNCRN, by using [29][Definition 4.7 and Proposition 4.9], which ensures that the equilibrium concentration of the fast (adjoined) system is globally stable.

B Appendix: Examples

In this section, we present some details underlying the examples from Section 4.

B.1 Multi-stable target system

Tri-stability. We use Algorithm 1 to approximate the target system (8) on $\mathbb{K}_1 = [1, 18]$. Tolerance $\varepsilon \approx 0.5 \times 10^{-3}$ is met with an RNCRN with $M = 4$ perceptrons, coefficients $\beta_1 = 0$, $\gamma = 1$, and

$$\boldsymbol{\alpha}_1 = \begin{pmatrix} -4.247 \\ 0.487 \\ 1.363 \\ 0.185 \end{pmatrix}, \quad \boldsymbol{\theta} = \begin{pmatrix} -4.968 \\ -3.590 \\ -11.236 \\ 10.249 \end{pmatrix}, \quad \boldsymbol{\omega}_1 = \begin{pmatrix} 0.511 \\ 1.043 \\ 1.078 \\ -2.355 \end{pmatrix}, \quad (26)$$

where $\boldsymbol{\alpha}_1 = (\alpha_{1,1}, \alpha_{1,2}, \alpha_{1,3}, \alpha_{1,4})^\top$, $\boldsymbol{\theta} = (\theta_1, \theta_2, \theta_3, \theta_4)^\top$, and $\boldsymbol{\omega}_1 = (\omega_{1,1}, \omega_{2,1}, \omega_{3,1}, \omega_{4,1})^\top$. The reduced ODE is given by

$$\frac{d\tilde{x}_1}{dt} = g_1(\tilde{x}_1) = \tilde{x}_1 \sum_{j=1}^4 \alpha_{1,j} \sigma_1(\omega_{j,1} \tilde{x}_1 + \theta_j), \quad (27)$$

while the full ODEs read

$$\begin{aligned} \frac{dx_1}{dt} &= x_1 \left(\sum_{j=1}^4 \alpha_{1,j} y_j \right), & x_1(0) &= a_1 \in \mathbb{K}_1, \\ \frac{dy_j}{dt} &= \frac{1}{\mu} + \frac{\theta_j}{\mu} y_j + \frac{\omega_{j,1}}{\mu} x_1 y_j - \frac{1}{\mu} y_j^2, & y_j(0) &= b_j \geq 0, \quad j = 1, 2, \dots, 4. \end{aligned} \quad (28)$$

Multi-stability. Analogous to Figure 2, we present some results for uni-, bi-, tri-, quad- and penta-stable RNCRNs in Figure 7(a)–(e). Furthermore, we present in Figure 7(f) the number of chemical perceptrons in the RNCRNs as a function of the number of the underlying stable equilibria, showing a linear trend; in particular, this plot suggests that $n + 1$ chemical perceptrons may be sufficient to achieve n stable equilibria. However, we note that the RNCRNs underlying Figure 7 are not necessarily the smallest ones achieved the indicated multi-stability.

B.2 Oscillatory target system

We use Algorithm 1 to approximate the target system (12) on $\mathbb{K}_1 \times \mathbb{K}_2 = [1, 8] \times [2, 10]$. Tolerance $\varepsilon \approx 10^{-4}$ is met with an RNCRN with $M = 6$ perceptrons and coefficients $\beta_1 = \beta_2 = 1$, $\gamma = 1$, and

$$\boldsymbol{\alpha}_1 = \begin{pmatrix} 0.664 \\ 3.392 \\ -1.159 \\ 10.658 \\ -2.799 \\ -0.571 \end{pmatrix}, \quad \boldsymbol{\alpha}_2 = \begin{pmatrix} 4.260 \\ 0.273 \\ -0.034 \\ 0.134 \\ -6.479 \\ -0.028 \end{pmatrix}, \quad \boldsymbol{\theta} = \begin{pmatrix} -1.833 \\ -2.452 \\ 8.979 \\ 2.420 \\ 0.344 \\ -6.624 \end{pmatrix}, \quad \boldsymbol{\omega}_1 = \begin{pmatrix} 0.290 \\ 0.466 \\ -2.195 \\ -1.584 \\ -0.2900 \\ 2.182 \end{pmatrix}, \quad \boldsymbol{\omega}_2 = \begin{pmatrix} -0.572 \\ 0.112 \\ -0.015 \\ -0.226 \\ -0.716 \\ 0.788 \end{pmatrix}, \quad (29)$$

where $\boldsymbol{\alpha}_i = (\alpha_{i,1}, \alpha_{i,2}, \dots, \alpha_{i,6})^\top$ for $i = 1, 2$, $\boldsymbol{\theta} = (\theta_1, \theta_2, \theta_3, \theta_4, \theta_5, \theta_6)^\top$, and $\boldsymbol{\omega}_k = (\omega_{1,k}, \omega_{2,k}, \dots, \omega_{6,k})^\top$ for $k = 1, 2$. The reduced ODEs are given by

$$\begin{aligned} \frac{d\tilde{x}_1}{dt} &= g_1(\tilde{x}_1, \tilde{x}_2) = 1 + \tilde{x}_1 \sum_{j=1}^6 \alpha_{1,j} \sigma_1(\omega_{j,1} \tilde{x}_1 + \omega_{j,2} \tilde{x}_2 + \theta_j), \\ \frac{d\tilde{x}_2}{dt} &= g_2(\tilde{x}_1, \tilde{x}_2) = 1 + \tilde{x}_2 \sum_{j=1}^6 \alpha_{2,j} \sigma_1(\omega_{j,1} \tilde{x}_1 + \omega_{j,2} \tilde{x}_2 + \theta_j), \end{aligned} \quad (30)$$

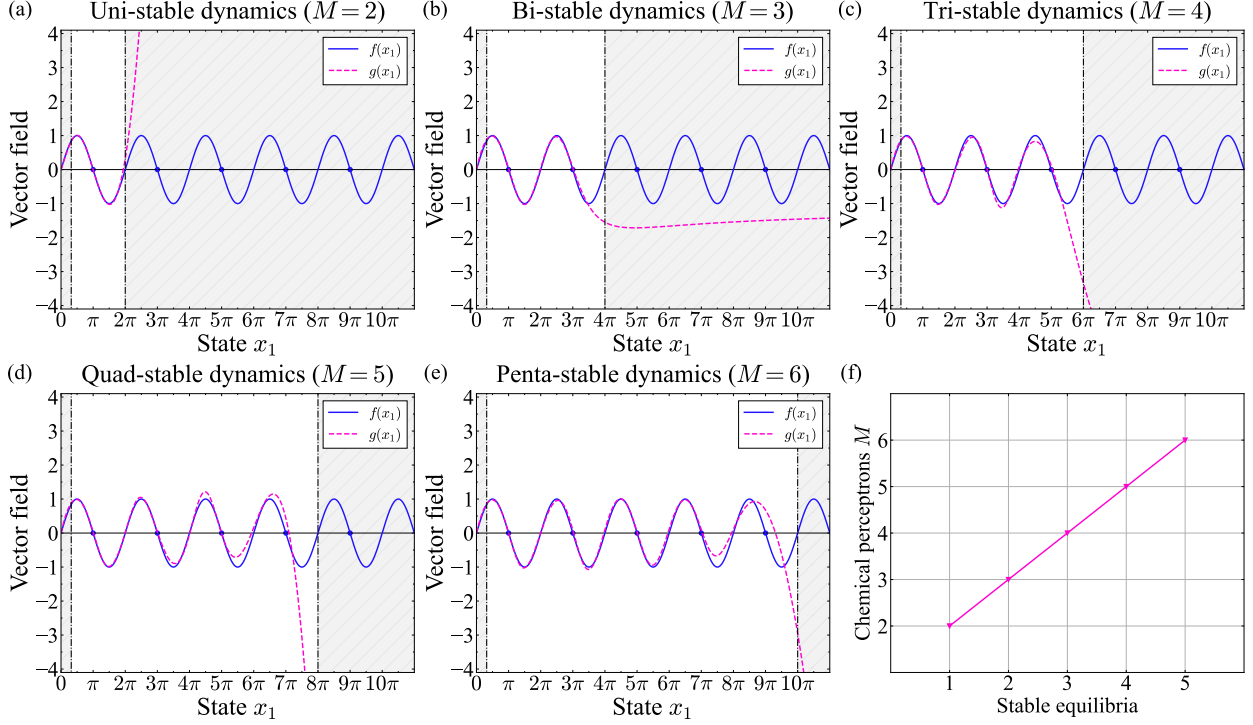


Figure 7: RNCRN approximations of the multi-stable target system (8). (a)-(e) The vector field of the target system (8) and reduced systems for some RNCRN trained over the following state-space sets: $\mathbb{K}_1 = [1, 2\pi]$ for uni-stability, $\mathbb{K}_1 = [1, 4\pi]$ for bi-stability, $\mathbb{K}_1 = [1, 6\pi]$ for tri-stability, $\mathbb{K}_1 = [1, 8\pi]$ for quad-stability, and $\mathbb{K}_1 = [1, 10\pi]$ for penta-stability. (f) Number of chemical perceptrons in the RNCRN as a function of the number of the underlying stable equilibria. The RNCRN are available in the code repository [83].

while the full ODEs read

$$\begin{aligned}
 \frac{dx_1}{dt} &= 1 + x_1 \left(\sum_{j=1}^6 \alpha_{1,j} y_j \right), & x_1(0) &= a_1 \in \mathbb{K}_1, \\
 \frac{dx_2}{dt} &= 1 + x_2 \left(\sum_{j=1}^6 \alpha_{2,j} y_j \right), & x_2(0) &= a_2 \in \mathbb{K}_2, \\
 \frac{dy_j}{dt} &= \frac{1}{\mu} + \frac{\theta_j}{\mu} y_j + \left(\sum_{i=1}^2 \frac{\omega_{j,i}}{\mu} x_i \right) y_j - \frac{1}{\mu} y_j^2, & y_j(0) &= b_j \geq 0, \quad j = 1, 2, \dots, 6.
 \end{aligned} \tag{31}$$

The coefficients were rounded to 3 decimal places before being used in simulations.

B.3 Chaotic target system

We use Algorithm 1 to approximate the target system (13) on $x_1 \in \mathbb{K}_1$, $x_2 \in \mathbb{K}_2$ and $x_3 \in \mathbb{K}_3$ with $\mathbb{K}_1 = \mathbb{K}_2 = \mathbb{K}_3 = [0.01, 1]$. Tolerance $\varepsilon \approx 10^2$ is met with an RNCRN with $M = 5$ perceptrons and

coefficients $\beta_1 = \beta_2 = \beta_3 = 0$, $\gamma = 1$, and

$$\begin{aligned} \boldsymbol{\alpha}_1 &= \begin{pmatrix} -0.272 \\ 2.996 \\ 0.862 \\ -0.244 \\ 1.276 \end{pmatrix}, \quad \boldsymbol{\alpha}_2 = \begin{pmatrix} 0.109 \\ 24.039 \\ -5.668 \\ -0.057 \\ -9.584 \end{pmatrix}, \quad \boldsymbol{\alpha}_3 = \begin{pmatrix} 0.026 \\ -0.529 \\ -1.101 \\ 0.034 \\ 1.065 \end{pmatrix}, \\ \boldsymbol{\theta} &= \begin{pmatrix} 0.284 \\ -1.589 \\ -0.178 \\ 1.212 \\ -0.707 \end{pmatrix}, \quad \boldsymbol{\omega}_1 = \begin{pmatrix} -5.049 \\ 0.148 \\ 0.506 \\ 15.973 \\ -1.151 \end{pmatrix}, \quad \boldsymbol{\omega}_2 = \begin{pmatrix} 8.895 \\ -2.951 \\ -4.504 \\ -7.781 \\ -0.606 \end{pmatrix}, \quad \boldsymbol{\omega}_3 = \begin{pmatrix} -0.068 \\ -0.525 \\ 0.329 \\ -0.027 \\ 0.199 \end{pmatrix}, \end{aligned} \quad (32)$$

where $\boldsymbol{\alpha}_i = (\alpha_{i,1}, \alpha_{i,2}, \dots, \alpha_{i,5})^\top$ for $i = 1, 2, 3$, $\boldsymbol{\theta} = (\theta_1, \theta_2, \theta_3, \theta_4, \theta_5)^\top$, and $\boldsymbol{\omega}_k = (\omega_{1,k}, \omega_{2,k}, \dots, \omega_{5,k})^\top$ for $k = 1, 2, 3$. The reduced ODEs are given by

$$\frac{d\tilde{x}_i}{dt} = g_i(\tilde{x}_1, \tilde{x}_2, \tilde{x}_3) = \tilde{x}_i \sum_{j=1}^5 \alpha_{i,j} \sigma_1 (\omega_{j,1} \tilde{x}_1 + \omega_{j,2} \tilde{x}_2 + \omega_{j,3} \tilde{x}_3 + \theta_j), \quad i = 1, 2, 3, \quad (33)$$

while the full ODEs read

$$\begin{aligned} \frac{dx_i}{dt} &= x_i \left(\sum_{j=1}^5 \alpha_{i,j} y_j \right), & x_i(0) &= a_i \in \mathbb{K}_i, \quad i = 1, 2, 3, \\ \frac{dy_j}{dt} &= \frac{1}{\mu} + \frac{\theta_j}{\mu} y_j + \left(\sum_{i=1}^3 \frac{\omega_{j,i}}{\mu} x_i \right) y_j - \frac{1}{\mu} y_j^2, & y_j(0) &= b_j \geq 0, \quad j = 1, 2, \dots, 5. \end{aligned} \quad (34)$$

The coefficients were rounded to 3 decimal places before being used in simulations.

C Appendix: DNA-strand-displacement implementation

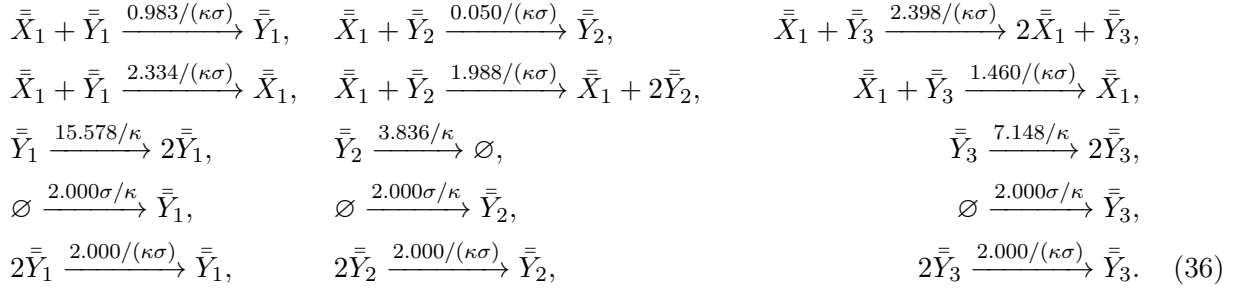
Let us consider the RREs (10), and assume now that the concentrations x_1, y_1, y_2, y_3 are measured in units of moles (M), while time t in units of seconds (s). In this section, we compile the induced RNCRN into a DNA-strand-displacement system with physically admissible rate coefficients (i.e. rate coefficients between $1M^{-1}s^{-1}$ to $10^6M^{-1}s^{-1}$) and admissible concentrations (i.e. concentrations less than $10^{-5}M$) [62]; to ensure these constraints, we fix the perceptron speed at a larger value, $\mu = 0.5$ in (10). Such DNA systems rely on suitable ‘‘fuel’’ species, which are depleted over time, being present at sufficiently high concentrations. To simplify analysis and simulations, one approach is to assume that the concentrations of the fuel species are held constant. This *constant-fuel assumption* [62] can be maintained *in situ* by additional experimental techniques that produce components [77, 78], increased buffering [87], or manually replenishing the fuel species at regular time-intervals. In the remainder of this section, we follow three steps: firstly, we introduce a suitable rescaled RNCRN; secondly, we map this network into a DNA-based RNCRN, and choose the rescaling such that its rate coefficients and species concentrations are admissible; finally, we simplify the latter network by making the constant-fuel assumption.

Rescaled RNCRN. Let us first rescale time and concentrations from RREs (10) by defining the new variables $\tau = \kappa t$, $\bar{x}_i(t) = \sigma x(t)$, $\bar{y}_i(t) = \sigma y_i(t)$ for $i = 1, 2, 3$ [62], where $\kappa, \sigma > 0$ are

dimensionless, and fix the dimensionless parameter $\mu = 0.5$, leading to the *rescaled* RREs:

$$\begin{aligned}
\frac{d\bar{x}_1}{d\tau} &= -\frac{0.983}{\kappa\sigma}\bar{x}_1\bar{y}_1 - \frac{0.050}{\kappa\sigma}\bar{x}_1\bar{y}_2 + \frac{2.398}{\kappa\sigma}\bar{x}_1\bar{y}_3, & \bar{x}_1(0) &= \sigma a_1, \\
\frac{d\bar{y}_1}{d\tau} &= 2\frac{\sigma}{\kappa} + \frac{15.578}{\kappa}\bar{y}_1 - \frac{2.334}{\kappa\sigma}\bar{x}_1\bar{y}_1 - \frac{2}{\kappa\sigma}\bar{y}_1^2, & \bar{y}_1(0) &= \sigma b_1, \\
\frac{d\bar{y}_2}{d\tau} &= 2\frac{\sigma}{\kappa} - \frac{3.836}{\kappa}\bar{y}_2 + \frac{1.988}{\kappa\sigma}\bar{x}_1\bar{y}_2 - \frac{2}{\kappa\sigma}\bar{y}_2^2, & \bar{y}_2(0) &= \sigma b_2, \\
\frac{d\bar{y}_3}{d\tau} &= 2\frac{\sigma}{\kappa} + \frac{7.148}{\kappa}\bar{y}_3 - \frac{1.460}{\kappa\sigma}\bar{x}_1\bar{y}_3 - \frac{2}{\kappa\sigma}\bar{y}_3^2, & \bar{y}_3(0) &= \sigma b_3.
\end{aligned} \tag{35}$$

Denoting the chemical species with the rescaled concentrations \bar{x}_1, \bar{y}_i by \bar{X}_1 and \bar{Y}_i , respectively, the *rescaled* RNCRN induced by (35) is given by



DNA-RNCRN. The rescaled RNCRN (36) can be mapped into a DNA-strand-displacement-based CRN [62], which we call the DNA-RNCRN, and present in the text files entitled “domain_level_DNA_full_inits” in the folder “ex_5_dna_implementation/CRNs” available in [83]. This network consists of 78 chemical species (representing single- and double-stranded DNAs), and 53 reactions, all of which involve exactly two reactants. We fix the scaling parameters to $\kappa = 3 \times 10^4$ and $\sigma = 5 \times 10^{-9}$; then, the underlying rate coefficients of all the chemical reactions in the DNA-RNCRN can be shown to be between $7M^{-1}s^{-1}$ and $10^6M^{-1}s^{-1}$, and the concentrations of all of the species are then less than $10^{-5}M$, i.e. within the physically admissible range. We show the concentration of the executive species $\bar{x}_1(t)$ from the DNA-RNCRN for various initial conditions as the red curves in Figure 8(a); also shown for comparison is the corresponding solution from the rescaled target system (35). One can notice that the DNA-RNCRN approximately displays the intended bistability for some interval of time. However, as time progresses further, some of the fuel species are significantly depleted and, consequently, the DNA-RNCRN starts to deviate significantly from its target behavior.

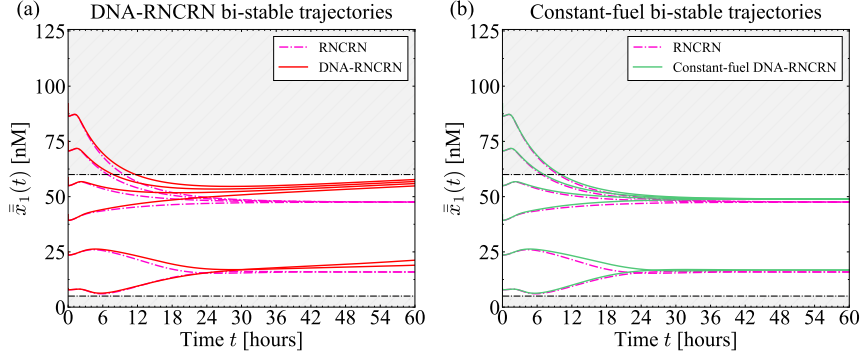


Figure 8: DNA-strand-displacement implementation of the RNCrN with RREs (10) with $\mu = 0.5$. Panel (a) shows in red the concentration of the executive species from the DNA-RNCrN, presented in [83]. Also shown in purple is the concentrations of the executive species from the RREs (35), with initial conditions $\bar{x}_1(0) \in \{7.85 \times 10^{-9} \text{ M}, 2.36 \times 10^{-8} \text{ M}, 3.93 \times 10^{-8} \text{ M}, 5.50 \times 10^{-8} \text{ M}, 7.07 \times 10^{-8} \text{ M}, 8.64 \times 10^{-8} \text{ M}\}$, and zero initial concentration for all chemical perceptrons. Analogous plot is shown in panel (b), where the green curve is the concentration of the executive species from the constant-fuel RNCrN (40), with initial conditions $\bar{x}_1(0) \in \{8.37 \times 10^{-9} \text{ M}, 2.51 \times 10^{-8} \text{ M}, 4.18 \times 10^{-8} \text{ M}, 5.86 \times 10^{-8} \text{ M}, 7.53 \times 10^{-8} \text{ M}, 9.20 \times 10^{-8} \text{ M}\}$, $C_{11}(0) = C_{12}(0) = C_{13}(0) = 5.33 \times 10^{-9} \text{ M}$, and all the other species having zero concentration initially. Note that, due to the buffering modules, initial conditions for the executive species from (36) and (40) are slightly different. The simulations were performed using the full precision stated in the associated text files.

In what follows, we outline how the DNA-RNCrN is designed; we abuse the notation slightly, by following the notation from [62].

Zero-order reactions. The abstract zero-order reaction (i.e. reaction with \emptyset as the reactants) of the form $\emptyset \xrightarrow{\gamma_i} \bar{Y}_i$ is mapped to the DNA-based network given by



where C_i , \bar{Y}_i , and O_i are single-stranded DNAs, while G_i and T_i are double-stranded DNA complexes called gates, acting as fuel species. Let us note that C_i plays an effectively catalytic role in this reaction cascade. The initial concentrations for the fuel species G_i and T_i are set to respectively $G_i(0) = 10^{-5} M$ and $T_i(0) = 10^{-5} M$. Furthermore, to ensure the effective reaction rate γ_i , we fix the initial condition of C_i to $C_i(0) = \delta M$; in particular, in the DNA-strand-displacement framework, effective rates of reactions are calibrated using the initial conditions of suitable DNA species.

First-order reactions. The abstract first-order reaction (i.e. reaction with only one reactant) of the form $\bar{Y}_i \xrightarrow{\theta_i} 2\bar{Y}_i$ is mapped to the DNA-based network given by



where \bar{Y}_i and O_i are single-stranded DNAs and, as before, G_i and T_i are fuel species with initial concentrations $G_i(0) = T_i(0) = 10^{-5} M$. A similar DNA-based network is designed for abstract reactions of the form $Y_i \xrightarrow{\theta_i} \emptyset$.

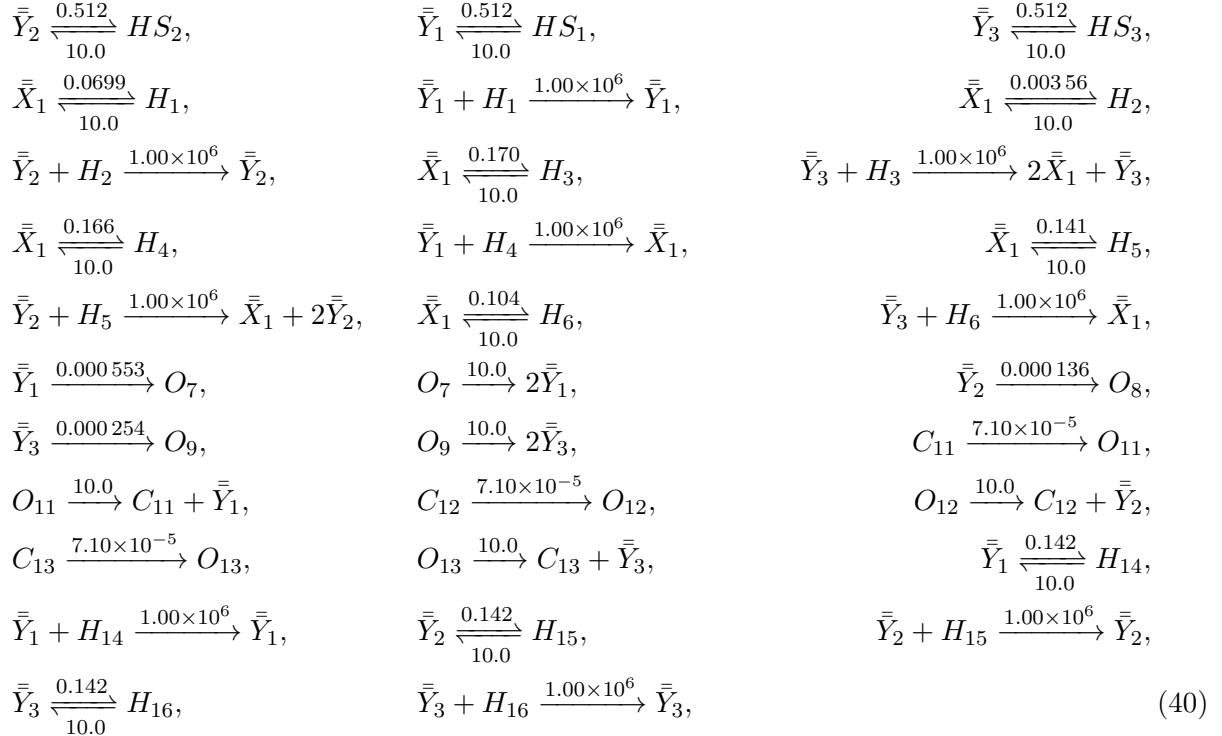
Second-order reactions. Finally, the abstract second-order reaction (i.e. reaction with two reactants) of the form $2\bar{Y}_i \xrightarrow{\kappa_i} \bar{Y}_i$ is mapped to the DNA-based network given by



where \bar{Y}_i , B_i , and O_i are single-stranded, while L_i , H_i , T_i double-stranded DNAs. The initial concentrations for the fuel species are set to $L_i(0) = T_i(0) = B_i(0) = 10^{-5}M$. Similar DNA-based networks are designed for the other variants of second-order reactions.

Buffering. We also introduce into the DNA-RNCRN the so-called buffering modules [62]. These modules require that certain rate coefficients and initial conditions are multiplied by a factor, which we account for in the presented results.

Constant-fuel DNA-RNCRN. To address the deviation of the DNA-RNCRN from its target behavior displayed in Figure 8(a), the fuel species must be replenished. In this paper, we do not model such replenishment explicitly; instead, for simplicity, we assume that the concentrations of all fuel species in the DNA-RNCRN are constant. Then, this network can be approximated [62] by the *constant-fuel* DNA-RNCRN, given by



with $C_{11}(0) = C_{12}(0) = C_{13}(0) = 5.33 \times 10^{-9}M$, while the initial conditions for all the other auxiliary species (i.e. all species except the executive species X_1 and chemical peregtrons Y_1, Y_2, Y_3) are set to zero. Let us note that the fuel species concentrations from the DNA-RNCRN, assumed to be fixed to constant $10^{-5}M$, are absorbed into effective rate coefficients displayed above the reaction arrows in (40). The concentration of the executive species $\bar{x}_1(t)$ from (40) is shown in Figure 3(b), which we repeat for convenience as Figure 8(b). One can observe that the constant-fuel DNA-RNCRN

displays the desired behavior which, owing to effective replenishment of the fuel species, is now maintained over the desired interval of time.

D Appendix: Robustness

In this section, we provide a preliminary investigation of robustness of some RNCRNs approximating the oscillatory target system (12). In particular, we first consider the RNCRN with RREs (31). This RNCRN was not optimized for robustness; nevertheless, we show that it is not pathologically sensitive to perturbations. We then apply a noisy version of Algorithm 1 on the target system (12) to produce a new oscillatory RNCRN which is more robust to perturbations.

D.1 Rate-coefficient robustness

Let us consider RREs (31) with perturbed rate coefficients and fixed perceptron speed μ , given by

$$\begin{aligned} \frac{d\hat{x}_i}{dt} &= \hat{\beta}_i + \hat{x}_i \sum_{j=1}^M \hat{\alpha}_{i,j} \hat{y}_j, & \hat{x}_i(0) &= a_i, \quad \text{for } i = 1, 2, \\ \frac{d\hat{y}_j}{dt} &= \frac{\hat{\gamma}}{\mu} + \frac{\hat{\theta}_j}{\mu} \hat{y}_j + \left(\sum_{i=1}^N \frac{\hat{\omega}_{j,i}}{\mu} \hat{x}_i \right) y_j - \frac{\hat{\kappa}_j}{\mu} \hat{y}_j^2, & \hat{y}_j(0) &= b_j, \quad \text{for } j = 1, 2, \dots, 6, \end{aligned} \quad (41)$$

with coefficients

$$\begin{aligned} \hat{\beta}_i &= 1 + \eta r_{\beta_i}, \quad \hat{\alpha}_{i,j} = (1 + \eta r_{\alpha_{i,j}}) \alpha_{i,j}, \quad \hat{\gamma} = 1 + \eta r_{\gamma}, \\ \hat{\omega}_{j,i} &= (1 + \eta r_{\omega_{j,i}}) \omega_{j,i}, \quad \hat{\theta}_j = (1 + \eta r_{\theta_j}) \theta_j, \quad \hat{\kappa}_i = 1 + \eta r_{\kappa_i}, \end{aligned} \quad (42)$$

where $r \in (-1, 1)$ with appropriate subscripts are independent uniformly distributed random variables, scaled with a parameter $\eta \in [0, 1]$, i.e. ηr is uniformly distributed in $[-\eta, \eta]$.

To study robustness, we fix the initial conditions to $a_1 = 2$, $a_2 = 4$ and $b_j = 0$, the perceptron speed to $\mu = 0.1$, and the noise strength to $\eta \in [0, 1]$. Then, for a fixed sampling of coefficients (42), we numerically solve the resulting perturbed RREs (41). We then verify if the solution $\hat{x}_1(t)$ is a periodic function of time within the time-interval $t \in [0, 60]$; if this is the case, then we say that RREs (31) are robust with respect to this particular set of perturbations. For this verification, we use a fast Fourier transform and check for the existence of suitable peaks, above a threshold, in the frequency domain (see code [83] for implementation). We then repeat this procedure for sufficiently many samplings of (42), and compute the ratio of oscillatory to non-oscillatory perturbed systems, which we use as an estimate for rate-coefficient robustness for fixed η . We then repeat the same computations for various values of noise strength $\eta \in [0, 1]$. See Figure 5(a)–(b).

D.2 Perceptron-speed robustness

To study robustness with respect to the parameter μ , we numerically solve the RREs (31) with rate coefficients (29) and various values of μ . The results are shown in Figure 5(c)–(d).

D.3 Initial-condition robustness

Let us now consider RREs (31) with perturbed initial conditions, given by

$$\begin{aligned} \frac{d\hat{x}_i}{dt} &= \beta_i + \hat{x}_i \sum_{j=1}^M \alpha_{i,j} \hat{y}_j, & \hat{x}_i(0) &= (1 + \eta r_{a_i}) a_i, \text{ for } i = 1, 2, \\ \frac{d\hat{y}_j}{dt} &= \frac{\gamma}{\mu} + \frac{\theta_j}{\mu} \hat{y}_j + \left(\sum_{i=1}^N \frac{\omega_{j,i}}{\mu} \hat{x}_i \right) y_j - \frac{\kappa_j}{\mu} \hat{y}_j^2, & \hat{y}_j(0) &= (1 + \eta r_{b_j}) b_j, \text{ for } j = 1, 2, \dots, 6, \end{aligned} \quad (43)$$

where $r \in (-1, 1)$ with appropriate subscripts are independent uniformly distributed random variables, and parameter $\eta \in [0, 1]$.

We fix the rate coefficients from (43) to (29) and $\mu = 0.1$. Furthermore, we fix $a_1 = 2$ and $a_2 = 4$, while b_j are fixed to the equilibrium values of the chemical perceptrons: $b_1 = 1.79$, $b_2 = 0.17$, $b_3 = 0.20$, $b_4 = 4.19$, $b_5 = 0.42$, and $b_6 = 1.22$. The results are presented in Figure 5(e)–(f).

D.4 Noisy training

The RNCRN with RREs (31) has been produced by applying Algorithm 1 with deterministic coefficients $\beta_i, \alpha_{i,j}, \gamma, \omega_{j,i}, \theta_j$ in (7). In order to design an RNCRN which is more robust to perturbations in the rate coefficients, one may wish to instead apply Algorithm 1 with coefficients $\beta_i, \alpha_{i,j}, \gamma, \omega_{j,i}, \theta_j$ being stochastically perturbed at each iteration of the backpropagation algorithm. For the purpose of this paper, instead of perturbing each of the coefficients, we introduce only three perturbations, which we choose in a way natural to our computer code. In particular, let us now consider Algorithm 1 with one modification: in step (a), we ensure that the distance between $(f_i(x_1, x_2, \dots, x_N)/x_i - \beta_i/x_i)$ and $\sum_{j=1}^M \alpha_{i,j}^* \left(\delta_j^{(y)} + \sigma_\gamma \left(\sum_{k=1}^N \omega_{j,k}^* (x_k + \delta_k^{(x)}) + \theta_j^* \right) \right) + \delta_i^{(\beta)}$ is within the tolerance, instead of $\sum_{j=1}^M \alpha_{i,j}^* \sigma_\gamma \left(\sum_{k=1}^N \omega_{j,k}^* x_k + \theta_j^* \right)$. Here, $\delta_k^{(x)}$, $\delta_j^{(y)}$, $\delta_i^{(\beta)}$ are independent normal random variables with zero mean and variance η^2 , which we prescribe. These three random variables are resampled at each iteration of the backpropagation algorithm. See the code presented in the folder entitled “step_4_noisy_training” within the folder “ex_6_robustness” available in [83].

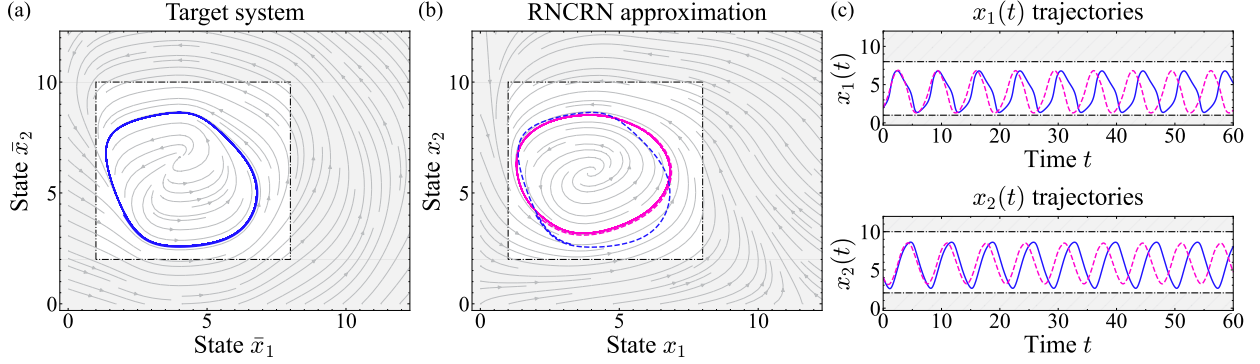


Figure 9: RNCRN approximation of the oscillatory target system (12) trained with noisy Algorithm 1. (a) The vector field of the target system (12) (grey arrows) for $\mathbb{K}_1 \times \mathbb{K}_2 = [1, 8] \times [2, 10]$, and a solution of (12) with $\bar{x}_1(0) = 2$ and $\bar{x}_2(0) = 4$ (blue). (b) Analogous plot is shown for the RNCRN whose reduced and full ODEs are given respectively by (45) and (46), with coefficients (44) and $\mu = 0.01$. In particular, displayed as grey arrows is the vector field of the reduced ODEs (45), together with an oscillatory solution of the full ODEs (46) shown in purple; for comparison, we also display as dashed blue curve the oscillatory solution of (12) from (a). Panel (c) displays the solutions $\bar{x}_1(t)$ and $x_1(t)$, and $\bar{x}_2(t)$ and $x_2(t)$. The initial concentrations of the perceptrons are all set to zero.

Applying this noisy version of Algorithm 1 to the target system (12) on $\mathbb{K}_1 \times \mathbb{K}_2 = [1, 8] \times [2, 10]$, with tolerance $\varepsilon \approx 10^{-1}$ and variance $\eta^2 = 1$, we find an RNCRN with $M = 6$ perceptrons, coefficients $\beta_1 = \beta_2 = 1$, $\gamma = 1$, and rounded to 3 decimal places:

$$\boldsymbol{\alpha}_1 = \begin{pmatrix} -0.034 \\ -0.040 \\ 0.017 \\ 0.036 \\ 0.037 \\ -0.011 \end{pmatrix}, \quad \boldsymbol{\alpha}_2 = \begin{pmatrix} 0 \\ -0.014 \\ -0.023 \\ -0.013 \\ 0.011 \\ 0.020 \end{pmatrix}, \quad \boldsymbol{\theta} = \begin{pmatrix} -18.748 \\ 34.068 \\ 39.575 \\ 36.980 \\ 49.304 \\ -1.085 \end{pmatrix}, \quad \boldsymbol{\omega}_1 = \begin{pmatrix} -2.101 \\ -7.724 \\ -5.370 \\ -1.695 \\ -13.497 \\ 5.802 \end{pmatrix}, \quad \boldsymbol{\omega}_2 = \begin{pmatrix} 5.662 \\ 0.522 \\ -4.331 \\ -3.996 \\ -3.471 \\ -3.901 \end{pmatrix}, \quad (44)$$

where $\boldsymbol{\alpha}_i = (\alpha_{i,1}, \alpha_{i,2}, \dots, \alpha_{i,6})^\top$ for $i = 1, 2$, $\boldsymbol{\theta} = (\theta_1, \theta_2, \theta_3, \theta_4, \theta_5, \theta_6)^\top$, and $\boldsymbol{\omega}_k = (\omega_{1,k}, \omega_{2,k}, \dots, \omega_{6,k})^\top$ for $k = 1, 2$. The reduced ODEs are given by

$$\begin{aligned} \frac{d\tilde{x}_1}{dt} &= g_1(\tilde{x}_1, \tilde{x}_2) = 1 + \tilde{x}_1 \sum_{j=1}^6 \alpha_{1,j} \sigma_1(\omega_{j,1}\tilde{x}_1 + \omega_{j,2}\tilde{x}_2 + \theta_j), \\ \frac{d\tilde{x}_2}{dt} &= g_2(\tilde{x}_1, \tilde{x}_2) = 1 + \tilde{x}_2 \sum_{j=1}^6 \alpha_{2,j} \sigma_1(\omega_{j,1}\tilde{x}_1 + \omega_{j,2}\tilde{x}_2 + \theta_j), \end{aligned} \quad (45)$$

while the full ODEs read

$$\begin{aligned}
\frac{dx_1}{dt} &= 1 + x_1 \left(\sum_{j=1}^6 \alpha_{1,j} y_j \right), & \hat{x}_1(0) &= a_1 \in \mathbb{K}_1, \\
\frac{dx_2}{dt} &= 1 + x_2 \left(\sum_{j=1}^6 \alpha_{2,j} y_j \right), & \hat{x}_2(0) &= a_2 \in \mathbb{K}_2, \\
\frac{dy_j}{dt} &= \frac{1}{\mu} + \frac{\theta_j}{\mu} y_j + \left(\sum_{i=1}^2 \frac{\omega_{j,i}}{\mu} x_i \right) y_j - \frac{1}{\mu} y_j^2, & y_j(0) &= b_j \geq 0, \quad j = 1, 2, \dots, 6.
\end{aligned} \tag{46}$$

We present the dynamics of (46) in Figure 9, which is analogous to Figure 4. Furthermore, in Figure 5(a), we show that this RNCRN displays superior robustness.

E Appendix: Alternative approximation scheme

In this section, we outline an alternative method for approximating non-polynomial ODEs with RREs [73, 74], and point out some of its drawbacks.

Non-polynomial to polynomial ODEs. Consider again the non-polynomial ODE (8). To map it to a polynomial one, we apply the method from [74]: we introduce the auxiliary variables $y_1 = \sin(x_1)$ and $y_2 = \cos(x_1)$, and use the chain-rule to obtain

$$\begin{aligned}
\frac{dx_1}{dt} &= y_1, & x_1(0) &= a_1, \\
\frac{dy_1}{dt} &= y_1 y_2, & y_1(0) &= \sin(a_1), \\
\frac{dy_2}{dt} &= -y_1^2, & y_2(0) &= \cos(a_1).
\end{aligned} \tag{47}$$

Polynomial ODEs to RREs. To ensure that the initial conditions for y_1 and y_2 are non-negative, we translate the variables according to $z_1(t) = T_1 + y_1(t)$ and $z_2(t) = T_2 + y_2(t)$, where $T_1, T_2 > 1$; for concreteness, we fix $T_1 = T_2 = 2$. Then, (47) becomes

$$\begin{aligned}
\frac{dx_1}{dt} &= -2 + z_1, & x_1(0) &= a_1, \\
\frac{dz_1}{dt} &= 4 - 2z_1 - 2z_2 + z_1 z_2, & z_1(0) &= 2 + \sin(a_1), \\
\frac{dz_2}{dt} &= -4 + 4z_1 - z_1^2, & z_2(0) &= 2 + \cos(a_1).
\end{aligned} \tag{48}$$

Terms -2 , $-2z_2$ and $-4 - z_1^2$ in respectively the first, second and third equation of (48) cannot be interpreted as chemical reactions [59]. Multiple methods exist to eliminate such non-chemical terms [59, 68–72]; in what follows, we use incomplete Carleman embedding [73]. In particular, introducing additional variables $z_3 = 1/x_1$, $z_4 = 1/z_1$, and $z_5 = 1/z_2$, and applying the chain-rule,

yields

$$\begin{aligned}
\frac{dx_1}{dt} &= -2x_1z_3 + z_1, & x_1(0) &= a_1, \\
\frac{dz_1}{dt} &= 4 - 2z_1 - 2z_1z_2z_4 + z_1z_2, & z_1(0) &= 2 + \sin(a_1), \\
\frac{dz_2}{dt} &= -4z_2z_5 + 4z_1 - z_1^2z_2z_5, & z_2(0) &= 2 + \cos(a_1), \\
\frac{dz_3}{dt} &= 2z_3^2 - z_1z_3^2, & z_3(0) &= \frac{1}{a_1}, \\
\frac{dz_4}{dt} &= 2z_4 - 4z_4^2 - z_2z_4 + 2z_2z_4^2, & z_4(0) &= \frac{1}{2 + \sin(a_1)}, \\
\frac{dz_5}{dt} &= 4z_5^2 - 4z_1z_5^2 + z_1^2z_5^2, & z_5(0) &= \frac{1}{2 + \cos(a_1)}. \tag{49}
\end{aligned}$$

RREs (49) contain terms of degree as high as four; for example, the term $-z_1^2z_2z_5$. This term induces the reaction $2Z_1 + Z_2 + Z_5 \xrightarrow{1} 2Z_1 + Z_5$, which has four reactants, and is therefore experimentally infeasible. One could approximate such higher-order reactions with systems of second-order ones [60,61]. However, for the purpose of this section, RREs (49) are sufficient.

Initial-condition robustness. Let us now numerically study robustness of (49) with respect to the initial conditions. In Figure 10(a), we display the solution $x_1(t)$ of (49), i.e. with ideal initial conditions. One can notice that $x_1(t)$ from (49) is *identical* to $\bar{x}_1(t)$ from the target system (8). However, note that this perfect accuracy requires one to perfectly adjust the initial conditions for the auxiliary species $z_i(0)$ for any given initial condition $x_i(0)$, i.e. if one changes $x_i(0)$, then one also has to appropriately change $z_i(0)$ for all $i = 1, 2, \dots, 5$. Critically, as we now show, this perfect accuracy can deteriorate catastrophically under some perturbations of the initial conditions.

In particular, let us consider (49) with perturbed initial conditions:

$$\begin{aligned}
\frac{d\hat{x}_1}{dt} &= -2\hat{x}_1\hat{z}_3 + \hat{z}_1, & \hat{x}_1(0) &= (1 + \eta r_1)a_1, \\
\frac{d\hat{z}_1}{dt} &= 4 - 2\hat{z}_1 - 2\hat{z}_1\hat{z}_2\hat{z}_4 + \hat{z}_1\hat{z}_2, & \hat{z}_1(0) &= (1 + \eta r_2)(2 + \sin(a_1)), \\
\frac{d\hat{z}_2}{dt} &= -4\hat{z}_2\hat{z}_5 + 4\hat{z}_1 - \hat{z}_1^2\hat{z}_2\hat{z}_5, & \hat{z}_2(0) &= (1 + \eta r_3)(2 + \cos(a_1)), \\
\frac{d\hat{z}_3}{dt} &= 2\hat{z}_3^2 - \hat{z}_1\hat{z}_3^2, & \hat{z}_3(0) &= (1 + \eta r_4)\frac{1}{a_1}, \\
\frac{d\hat{z}_4}{dt} &= 2\hat{z}_4 - 4\hat{z}_4^2 - \hat{z}_2\hat{z}_4 + 2\hat{z}_2\hat{z}_4^2, & \hat{z}_4(0) &= (1 + \eta r_5)\frac{1}{2 + \sin(a_1)}, \\
\frac{d\hat{z}_5}{dt} &= 4\hat{z}_5^2 - 4\hat{z}_1\hat{z}_5^2 + \hat{z}_1^2\hat{z}_5^2, & \hat{z}_5(0) &= (1 + \eta r_6)\frac{1}{2 + \cos(a_1)}, \tag{50}
\end{aligned}$$

where, as in Appendix D.3, $r_i \in (-1, 1)$ are independent uniformly distributed random variables, and parameter $\eta \in [0, 1]$. In the top panel of Figure 10(b), we show as a function of η the proportion of perturbed systems (50), over a range of initial conditions, whose solutions $x_1(t)$ converge to within $\pm\pi/4$ of the intended equilibrium; one can notice an increasing fragility beyond $\eta = 10\%$. Critically, for some non-ideal initial conditions, concentrations of some of the auxiliary species grow unboundedly (blow-up), as shown in the bottom panel of Figure 10(b). Let us note that no such chemically hazardous behavior is observed in the RNCRN. In Figure 10(c), we display a particular data point from Figure 10(b), showing that $x_1(t)$ from (50) can fail to converge close to the intended equilibrium π , while, at the same time, the auxiliary species concentration $z_5(t)$ blows up.

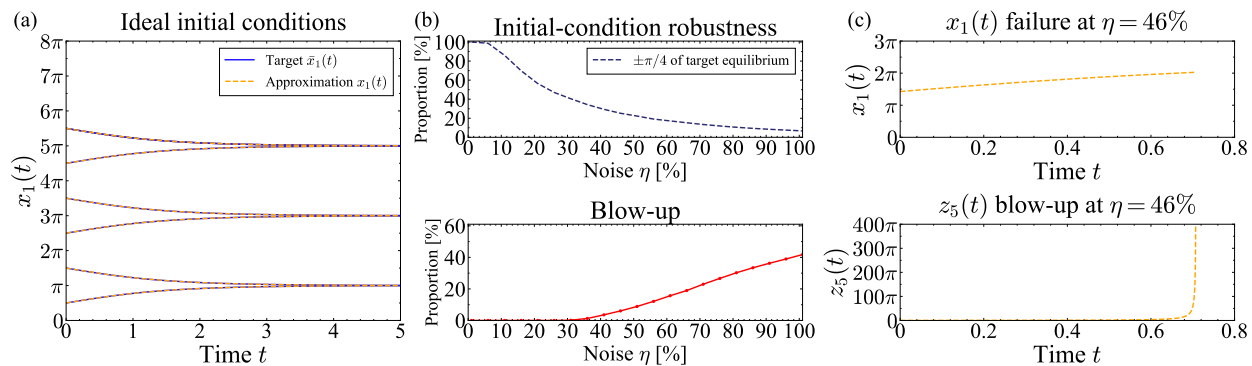


Figure 10: Initial-condition sensitivity of system (49) that approximates target system (8). Panel (a) shows solution $\bar{x}_1(t)$ of (8), and $x_1(t)$ of (49). Top sub-panel (b) shows the proportion of perturbed systems (50), over a range of initial conditions, whose solutions $x_1(t)$ are within $\pm\pi/4$ of the desired equilibrium at $t = 6$ as a function of noise strength η . Bottom sub-panel (b) shows the proportion of (50) with at least one auxiliary species that blows up before $t = 6$. Each point in panel (b) was obtained by simulating (50) with 10^4 sampled initial conditions. Panel (c) shows an example of failure of $x_1(t)$ to converge close to the desired equilibrium, and a blow-up of an auxiliary species. The initial conditions are as follows: $x_1(t) = 4.48121513$, $z_1(0) = 4.13072385$, $z_2(0) = 1.55830895$, $z_3(0) = 0.08109365$, $z_4(0) = 0.22538005$, $z_5(0) = 0.56915378$.

F Appendix: Algorithm 1 pseudocode

Algorithm 1 Two-step algorithm for training the RNCRN

Require: $f_i(\bar{x}_1, \dots, \bar{x}_N)$ for $i = 1, 2, \dots, N$ ▷ target system (5)
Require: $\mathbb{K}_1, \mathbb{K}_2, \dots, \mathbb{K}_N \subset (0, +\infty)$ ▷ target compact sets
Require: $\gamma > 0$ and $\beta_1, \beta_2, \dots, \beta_N \geq 0$ ▷ positive and nonnegative rate coefficients
Require: $\varepsilon_Q > 0$ and $\varepsilon_D > 0$ ▷ quasi-static and dynamical tolerance
Require: \mathcal{L}_Q and \mathcal{L}_D ▷ loss functions for the quasi-static and the dynamic approximation
Require: $T > 0$ ▷ time length of dynamics
Require: $a_1, a_2, \dots, a_M, b_1, b_2, \dots, b_M \geq 0$ ▷ initial conditions of target system
Require: $0 < \mu \ll 1$ ▷ speed of chemical perceptrons lower bound
Require: INTEGRATE($\mathbf{f}, t \in [0, T], \mathbf{z}(0)$) ▷ procedure for numerical integration
Require: MINIMIZE(\mathcal{L}, Ω) ▷ procedure to minimize loss (*i.e.* backpropagation [65])
Require: REDUCE(μ) ▷ procedure to reduce μ^* and ε_Q

procedure QUASI-STATIC APPROXIMATION(ε_Q)
 $M \leftarrow 0$
 $\varepsilon_Q^* \leftarrow \infty$
while $\varepsilon_Q^* > \varepsilon_Q$ **do**
 $M \leftarrow M + 1$
 $\mathcal{L} \leftarrow \mathcal{L}_Q \left\{ f_i(x_1, x_2, \dots, x_N)/x_i - \beta_i/x_i, \sum_{j=1}^M \alpha_{i,j} \sigma_\gamma \left(\sum_{k=1}^N \omega_{j,k} x_k + \theta_j \right) \right\}$
 $\varepsilon_Q^*, \alpha_{i,j}^*, \omega_{j,k}^*, \theta_j^* \leftarrow \text{MINIMIZE}(\mathcal{L}, (\alpha_{i,j}, \omega_{j,k}, \theta_j))$
end while
return $\varepsilon_Q^*, \alpha_{i,j}^*, \omega_{j,k}^*, \theta_j^*$
end procedure

procedure DYNAMICAL APPROXIMATION(ε_Q)
 $\varepsilon_D^* \leftarrow \infty$
 $\mu^* \leftarrow 1$
 $\bar{\mathbf{z}}(0) \leftarrow (a_1, a_2, \dots, a_M)$
 $\mathbf{z}(0) \leftarrow (a_1, a_2, \dots, a_M, b_1, b_2, \dots, b_M)$
TARGET \leftarrow Equation (5)
 $\bar{x}_1(t), \dots, \bar{x}_N(t) \leftarrow \text{INTEGRATE}(\mathbf{TARGET}, t \in [0, T], \bar{\mathbf{z}}(0))$
 $\varepsilon_Q^*, \alpha_{i,j}^*, \omega_{j,k}^*, \theta_j^* \leftarrow \text{QUASI-STATIC APPROXIMATION}(\varepsilon_Q)$
while $\varepsilon_D^* > \varepsilon_D$ and $\mu^* > \mu$ **do**
 $\mu^* \leftarrow \text{REDUCE}(\mu^*)$
RNCRN \leftarrow Equation (6) with $\alpha_{i,j} = \alpha_{i,j}^*, \theta_j = \theta_j^*, \omega_{j,i} = \omega_{j,i}^*, \gamma, \mu^*$, and $\beta_1, \beta_2, \dots, \beta_N$
 $x_1(t), \dots, x_N(t), y_1(t), \dots, y_M(t) \leftarrow \text{INTEGRATE}(\mathbf{RNCRN}, t \in [0, T], \mathbf{z}(0))$
 $\varepsilon_D^* \leftarrow \mathcal{L}_D\{x_i(t), \bar{x}_i(t)\}$ over all $t \in [0, T]$ and all $i = 1, 2, \dots, N$
end while
if $\varepsilon_D^* < \varepsilon_D$ **then**
return $\alpha_{i,j}^*, \omega_{j,k}^*, \theta_j^*, \mu^*$
else
 $\varepsilon_Q \leftarrow \text{REDUCE}(\varepsilon_Q)$
return DYNAMICAL APPROXIMATION(ε_Q) ▷ recursive procedure
end if
end procedure
